# Transits and Occultations

## Joshua N. Winn

Massachusetts Institute of Technology

When we are fortunate enough to view an exoplanetary system nearly edge-on, the star and planet periodically eclipse each other. Observations of eclipses—transits and occultations—provide a bonanza of information that cannot be obtained from radial-velocity data alone, such as the relative dimensions of the planet and its host star, as well as the orientation of the planet's orbit relative to the sky plane and relative to the stellar rotation axis. The wavelength-dependence of the eclipse signal gives clues about the the temperature and composition of the planetary atmosphere. Anomalies in the timing or other properties of the eclipses may betray the presence of additional planets or moons. Searching for eclipses is also a productive means of discovering new planets. This chapter reviews the basic geometry and physics of eclipses, and summarizes the knowledge that has been gained through eclipse observations, as well as the information that might be gained in the future.

arXiv:1001.2010v5 [astro-ph.EP] 24 Sep 2014

## 1. INTRODUCTION

*From immemorial antiquity, men have dreamed of a royal road to success—leading directly and easily to some goal that could be reached otherwise only by long approaches and with weary toil. Times beyond number, this dream has proved to be a delusion.... Nevertheless, there are ways of approach to unknown territory which lead surprisingly far, and repay their followers richly. There is probably no better example of this than eclipses of heavenly bodies.* — Henry Norris Russell (1948)

Vast expanses of scientific territory have been traversed by exploiting the occasions when one astronomical body shadows another. The timing of the eclipses of Jupiter's moons gave the first accurate measure of the speed of light. Observing the passage of Venus across the disk of the Sun provided a highly refined estimate of the astronomical unit. Studying solar eclipses led to the discovery of helium, the recognition that Earth's rotation is slowing down due to tides, and the confirmation of Einstein's prediction for the gravitational deflection of light. The analysis of eclipsing binary stars—the subject Russell had in mind—enabled a precise understanding of stellar structure and evolution.

Continuing in this tradition, eclipses are the "royal road" of exoplanetary science. We can learn intimate details about exoplanets and their parent stars through observations of their combined light, without the weary toil of spatially resolving the planet and the star (see Figure 1). This chapter shows how eclipse observations are used to gain knowledge of the planet's orbit, mass, radius, temperature, and atmospheric constituents, along with other details that are otherwise hidden. This knowledge, in turn, gives clues about the processes of planet formation and evolution and provides a larger context for understanding the properties of the solar system.

An *eclipse* is the obscuration of one celestial body by another. When the bodies have very unequal sizes, the passage of the smaller body in front of the larger body is a *transit* and the passage of the smaller body behind the larger body is an *occultation*. Formally, transits are cases when the full disk of the smaller body passes completely within that of the larger body, and occultations refer to the complete concealment of the smaller body. We will allow those terms to include the *grazing* cases in which the bodies' silhouettes do not overlap completely. Please be aware that the exoplanet literature often refers to occultations as *secondary eclipses* (a more general term that does not connote an extreme size ratio), or by the neologisms "secondary transit" and "anti-transit."

This chapter is organized as follows. Section 2 describes the geometry of eclipses and provides the foundational equations, building on the discussion of Keplerian orbits in the chapter by Murray and Correia. Readers seeking a more elementary treatment involving only circular orbits may prefer to start by reading Sackett (1999). Section 3 discusses many scientific applications of eclipse data, including the determination of the mass and radius of the planet. Section 4 is a primer on observing the apparent decline in stellar brightness during eclipses (the *photometric* signal). Section 5 reviews some recent scientific accomplishments, and Section 6 offers some thoughts on future prospects.

## 2. ECLIPSE BASICS

### 2.1 Geometry of eclipses

Consider a planet of radius $R_p$ and mass $M_p$ orbiting a star of radius $R_\star$ and mass $M_\star$. The ratio $R_p/R_\star$ occurs frequently enough to deserve its own symbol, for which we will use $k$, in deference to the literature on eclipsing binary stars. As in the chapter by Murray and Correia, we choose a coordinate system centered on the star, with the sky in the $X$–$Y$ plane and the $+Z$ axis pointing at the observer (see Figure 2). Since the orientation of the line of nodes relative to celestial north (or any other externally defined axis) is usually unknown and of limited interest, we might
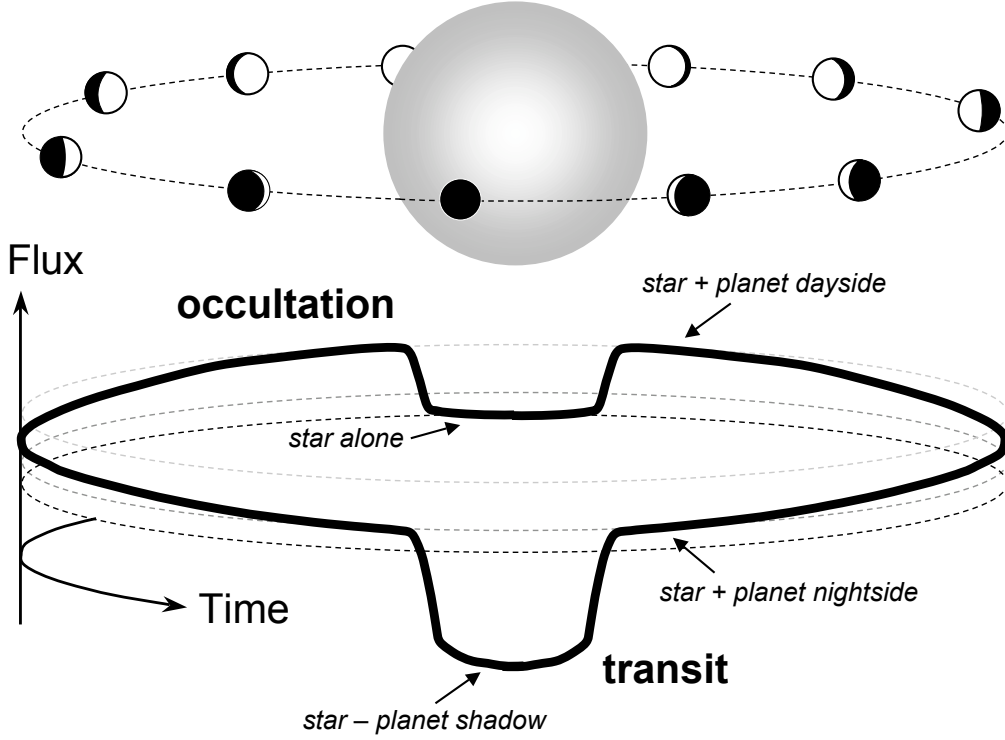
Fig. 1.— Illustration of transits and occultations. Only the combined flux of the star and planet is observed. During a transit, the flux drops because the planet blocks a fraction of the starlight. Then the flux rises as the planet's dayside comes into view. The flux drops again when the planet is occulted by the star.

as well align the $X$ axis with the line of nodes; we place the descending node of the planet's orbit along the $+X$ axis, giving $\Omega = 180°$.

The distance between the star and planet is given by equation (20) of the chapter by Murray and Correia:

$$r = \frac{a(1 - e^2)}{1 + e \cos f}, \tag{1}$$

where $a$ is the semimajor axis of the relative orbit and $f$ is the true anomaly, an implicit function of time depending on the orbital eccentricity $e$ and period $P$ (see Section 3 of the chapter by Murray and Correia). This can be resolved into Cartesian coordinates using equations (53-55) of the chapter by Murray and Correia, with $\Omega = 180°$:

$$X = -r \cos(\omega + f), \tag{2}$$
$$Y = -r \sin(\omega + f) \cos i, \tag{3}$$
$$Z = r \sin(\omega + f) \sin i. \tag{4}$$

If eclipses occur, they do so when $r_{\text{sky}} \equiv \sqrt{X^2 + Y^2}$ is a local minimum. Using equations (2-3),

$$r_{\text{sky}} = \frac{a(1 - e^2)}{1 + e \cos f} \sqrt{1 - \sin^2(\omega + f) \sin^2 i}. \tag{5}$$

Minimizing this expression leads to lengthy algebra (Kipping 2008). However, an excellent approximation that we will use throughout this chapter is that eclipses are centered around *conjunctions*, which are defined by the condition $X = 0$ and may be *inferior* (planet in front) or *superior* (star in front). This gives

$$f_{\text{tra}} = +\frac{\pi}{2} - \omega, \quad f_{\text{occ}} = -\frac{\pi}{2} - \omega, \tag{6}$$

where here and elsewhere in this chapter, "tra" refers to transits and "occ" to occultations. This approximation is valid for all cases except extremely eccentric and close-in orbits with grazing eclipses.

The *impact parameter* $b$ is the sky-projected distance at conjunction, in units of the stellar radius:

$$b_{\text{tra}} = \frac{a \cos i}{R_\star} \left( \frac{1 - e^2}{1 + e \sin \omega} \right), \tag{7}$$

$$b_{\text{occ}} = \frac{a \cos i}{R_\star} \left( \frac{1 - e^2}{1 - e \sin \omega} \right). \tag{8}$$

For the common case $R_\star \ll a$, the planet's path across (or behind) the stellar disk is approximately a straight line between the points $X = \pm R_\star \sqrt{1 - b^2}$ at $Y = b R_\star$.

### 2.2 Probability of eclipses

Eclipses are seen only by privileged observers who view a planet's orbit nearly edge-on. As the planet orbits its star, its shadow describes a cone that sweeps out a band on the celestial sphere, as illustrated in Figure 3. A distant observer within the shadow band will see transits. The opening angle of the cone, $\Theta$, satisfies the condition $\sin \Theta =$
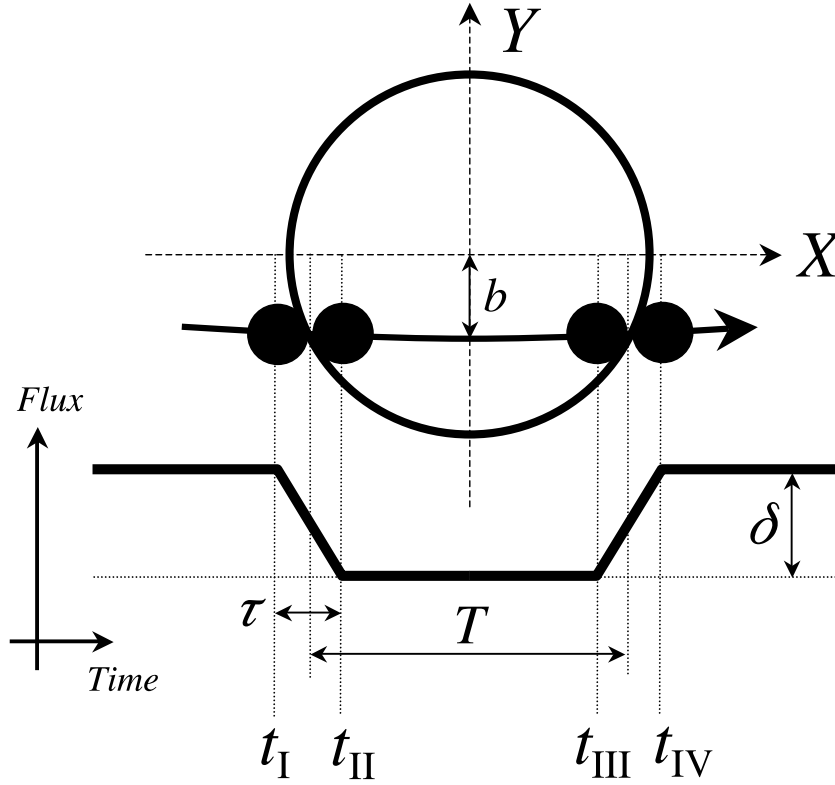
Fig. 2.— Illustration of a transit, showing the coordinate system discussed in Section 2.1, the four contact points and the quantities $T$ and $\tau$ defined in Section 2.3, and the idealized light curve discussed in Section 2.4.

$(R_\star + R_p)/r$ where $r$ is the instantaneous star-planet distance. This cone is called the *penumbra*. There is also an interior cone, the *antumbra*, defined by $\sin\Theta = (R_\star - R_p)/r$, inside of which the transits are full (non-grazing).

A common situation is that $e$ and $\omega$ are known and $i$ is unknown, as when a planet is discovered via the Doppler method (see chapter by Lovis and Fischer) but no information is available about eclipses. With reference to Figure 3, the observer's celestial longitude is specified by $\omega$, but the latitude is unknown. The transit probability is calculated as the shadowed fraction of the line of longitude, or more simply from the requirement $|b| < 1 + k$, using equations (7-8) and the knowledge that $\cos i$ is uniformly distributed for a randomly-placed observer. Similar logic applies to occultations, leading to the results

$$p_{\text{tra}} = \left(\frac{R_\star \pm R_p}{a}\right)\left(\frac{1 + e\sin\omega}{1 - e^2}\right), \qquad (9)$$

$$p_{\text{occ}} = \left(\frac{R_\star \pm R_p}{a}\right)\left(\frac{1 - e\sin\omega}{1 - e^2}\right), \qquad (10)$$

where the "+" sign allows grazing eclipses and the "−" sign excludes them. It is worth committing to memory the results for the limiting case $R_p \ll R_\star$ and $e = 0$:

$$p_{\text{tra}} = p_{\text{occ}} = \frac{R_\star}{a} \approx 0.005\left(\frac{R_\star}{R_\odot}\right)\left(\frac{a}{1\,\text{AU}}\right)^{-1}. \quad (11)$$

For a circular orbit, transits and occultations always go together, but for an eccentric orbit it is possible to see transits without occultations or vice versa.

In other situations, one may want to marginalize over all possible values of $\omega$, as when forecasting the expected number of transiting planets to be found in a survey (see Section 4.1) or other statistical calculations. Here, one can calculate the solid angle of the entire shadow band and divide by $4\pi$, or average equations (9-10) over $\omega$, giving

$$p_{\text{tra}} = p_{\text{occ}} = \left(\frac{R_\star \pm R_p}{a}\right)\left(\frac{1}{1 - e^2}\right). \quad (12)$$

Suppose you want to find a transiting planet at a particular orbital distance around a star of a given radius. If a fraction $\eta$ of stars have such planets, you must search at least $N \approx (\eta\,p_{\text{tra}})^{-1}$ stars before expecting to find a transiting planet. A sample of $>200\,\eta^{-1}$ Sun-like stars is needed to find a transiting planet at 1 AU. Close-in giant planets have an orbital distance of approximately 0.05 AU and $\eta \approx 0.01$, giving $N > 10^3$ stars. In practice, many other factors affect the survey requirements, such as measurement precision, time sampling, and the need for spectroscopic follow-up observations (see Section 4.1).

### 2.3 Duration of eclipses

In a non-grazing eclipse, the stellar and planetary disks
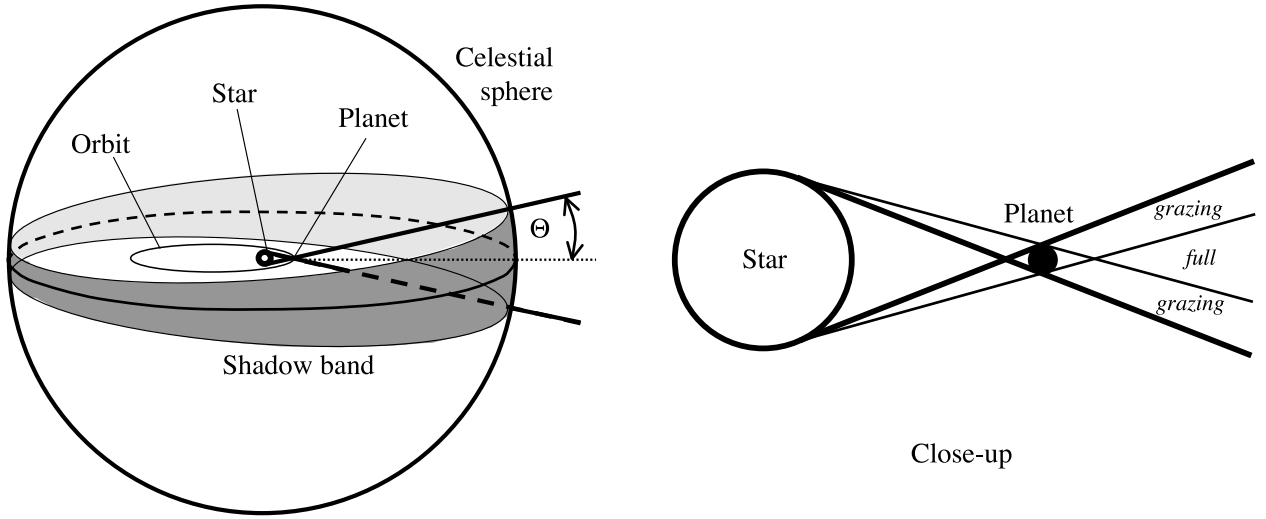
Fig. 3.— Calculation of the transit probability. *Left.*—Transits are visible by observers within the penumbra of the planet, a cone with opening angle $\Theta$ with $\sin \Theta = (R_\star + R_p)/r$, where $r$ is the instantaneous star-planet distance. *Right.*—Close-up showing the penumbra (thick lines) as well as the antumbra (thin lines) within which the transits are full, as opposed to grazing.

are tangent at four *contact times* $t_I$–$t_{IV}$, illustrated in Figure 2. (In a grazing eclipse, second and third contact do not occur.) The *total* duration is $T_{tot} = t_{IV} - t_I$, the *full* duration is $T_{full} = t_{III} - t_{II}$, the *ingress* duration is $\tau_{ing} = t_{II} - t_I$, and the *egress* duration is $\tau_{egr} = t_{IV} - t_{III}$.

Given a set of orbital parameters, the various eclipse durations can be calculated by setting equation (5) equal to $R_\star \pm R_p$ to find the true anomaly at the times of contact, and then integrating equation (44) of the chapter by Murray and Correia, e.g.,

$$t_{III} - t_{II} = \frac{P}{2\pi\sqrt{1-e^2}} \int_{f_{II}}^{f_{III}} \left[\frac{r(f)}{a}\right]^2 df. \qquad (13)$$

For a circular orbit, some useful results are

$$T_{tot} \equiv t_{IV} - t_I = \frac{P}{\pi} \sin^{-1}\left[\frac{R_\star}{a}\frac{\sqrt{(1+k)^2 - b^2}}{\sin i}\right], \qquad (14)$$

$$T_{full} \equiv t_{III} - t_{II} = \frac{P}{\pi} \sin^{-1}\left[\frac{R_\star}{a}\frac{\sqrt{(1-k)^2 - b^2}}{\sin i}\right]. \qquad (15)$$

For eccentric orbits, good approximations are obtained by multiplying equations (14-15) by

$$\frac{\dot{X}(f_c)\,[e=0]}{\dot{X}(f_c)} = \frac{\sqrt{1-e^2}}{1 \pm e \sin \omega}, \qquad (16)$$

a dimensionless factor to account for the altered speed of the planet at conjunction. Here, "+" refers to transits and "−" to occultations. One must also compute $b$ using the eccentricity-dependent equations (7-8).

For an eccentric orbit, $\tau_{ing}$ and $\tau_{egr}$ are generally unequal because the projected speed of the planet varies between

ingress and egress. In practice the difference is slight; to leading order in $R_\star/a$ and $e$,

$$\frac{\tau_e - \tau_i}{\tau_e + \tau_i} \sim e \cos \omega \left(\frac{R_\star}{a}\right)^3 (1-b^2)^{3/2}, \qquad (17)$$

which is $<10^{-2}\,e$ for a close-in planet with $R_\star/a = 0.2$, and even smaller for more distant planets. For this reason we will use a single symbol $\tau$ to represent either the ingress or egress duration. Another important timescale is $T \equiv T_{tot} - \tau$, the interval between the halfway points of ingress and egress (sometimes referred to as contact times 1.5 and 3.5).

In the limits $e \to 0$, $R_p \ll R_\star \ll a$, and $b \ll 1 - k$ (which excludes near-grazing events), the results are greatly simplified:

$$T \approx T_0 \sqrt{1-b^2}, \quad \tau \approx \frac{T_o k}{\sqrt{1-b^2}}, \qquad (18)$$

where $T_0$ is the characteristic time scale

$$T_0 \equiv \frac{R_\star P}{\pi a} \approx 13\,\text{hr}\,\left(\frac{P}{1\,\text{yr}}\right)^{1/3}\left(\frac{\rho_\star}{\rho_\odot}\right)^{-1/3}. \qquad (19)$$

For eccentric orbits, the additional factor given by equation (16) should be applied. Note that in deriving equation (19), we used Kepler's third law and the approximation $M_p \ll M_\star$ to rewrite the expression in terms of the stellar mean density $\rho_\star$. This is a hint that eclipse observations give a direct measure of $\rho_\star$, a point that is made more explicit in Section 3.1.

## 2.4 Loss of light during eclipses

The combined flux $F(t)$ of a planet and star is plotted in Figure 1. During a transit, the flux drops because the

4

planet blocks a fraction of the starlight. Then the flux rises as the planet's dayside comes into view. The flux drops again when the planet is occulted by the star. Conceptually we may dissect $F(t)$ as

$$F(t) = F_\star(t) + F_p(t) - \begin{cases} k^2\alpha_{\mathrm{tra}}(t)F_\star(t) & \text{transits,} \\ 0 & \text{outside eclipses,} \\ \alpha_{\mathrm{occ}}(t)F_p(t) & \text{occultations.} \end{cases} \tag{20}$$

where $F_\star, F_p$ are the fluxes from the stellar and planetary disks, and the $\alpha$'s are dimensionless functions of order unity depending on the overlap area between the stellar and planetary disks. In general $F_\star$ may vary in time due to flares, rotation of star spots and plages, rotation of the tidal bulge raised by the planet, or other reasons, but for simplicity of discussion we take it to be a constant. In that case, only the ratio $f(t) \equiv F(t)/F_\star$ is of interest. If we let $I_p$ and $I_\star$ be the disk-averaged intensities of the planet and star, respectively, then $F_p/F_\star = k^2 I_p/I_\star$ and

$$f(t) = 1 + k^2\frac{I_p(t)}{I_\star} - \begin{cases} k^2\alpha_{\mathrm{tra}}(t) & \text{transits,} \\ 0 & \text{outside eclipses,} \\ k^2\frac{I_p(t)}{I_\star}\alpha_{\mathrm{occ}}(t) & \text{occultations.} \end{cases} \tag{21}$$

Time variations in $I_p$ are caused by the changing illuminated fraction of the planetary disk (its *phase function*), as well as any changes intrinsic to the planetary atmosphere. To the extent that $I_p$ is constant over the relatively short timespan of a single eclipse, all of the observed time variation is from the $\alpha$ functions. As a starting approximation the $\alpha$'s are trapezoids, and $f(t)$ is specified by the depth $\delta$, duration $T$, ingress or egress duration $\tau$, and time of conjunction $t_c$, as shown in Figure 2. For transits the maximum loss of light is

$$\delta_{\mathrm{tra}} \approx k^2\left[1 - \frac{I_p(t_{\mathrm{tra}})}{I_\star}\right], \tag{22}$$

and in the usual case when the light from the planetary nightside is negligible, $\delta_{\mathrm{tra}} \approx k^2$. For occultations,

$$\delta_{\mathrm{occ}} \approx k^2\frac{I_p(t_{\mathrm{occ}})}{I_\star}. \tag{23}$$

In the trapezoidal approximation the flux variation during ingress and egress is linear in time. In reality this is not true, partly because of the nonuniform motion of the stellar and planetary disks. More importantly, even with uniform motion the overlap area between the disks is not a linear function of time [see equation (1) of Mandel & Agol (2002)]. In addition, the bottom of a transit light curve is not flat because real stellar disks do not have uniform intensity, as explained in the next section.

### 2.5 Limb darkening

Real stellar disks are brighter in the middle and fainter at the edge (the limb), a phenomenon known as *limb darkening*. This causes the flux decline during a transit to be larger than $k^2$ when the planet is near the center of the star, and smaller than $k^2$ when the planet is near the limb. The effect on the light curve is to round off the bottom and blur the 2nd and 3rd contact points, as shown in Figure 4. Limb darkening is a consequence of variations in temperature and opacity with altitude in the stellar atmosphere. The sightline to the limb follows a highly oblique path into the stellar atmosphere, and therefore an optical depth of unity is reached at a higher altitude, where the temperature is cooler and the radiation is less intense. The resulting intensity profile $I(X, Y)$ is often described with a fitting formula such as

$$I \propto 1 - u_1(1 - \mu) - u_2(1 - \mu)^2, \tag{24}$$

where $\mu \equiv \sqrt{1 - X^2 - Y^2}$ and $\{u_1, u_2\}$ are constant coefficients that may be calculated from stellar-atmosphere models or measured from a sufficiently precise transit light curve. The decision to use the quadratic function of equation (24) or another of the various limb-darkening "laws" (better described as fitting formulas) is somewhat arbitrary. Claret (2004) provides a compilation of theoretical coefficients, and advocates a four-parameter law. Southworth (2008) investigates the results of fitting the same data set with different limb-darkening laws. Mandel & Agol (2002) give accurate expressions for $\alpha_{\mathrm{tra}}(t)$ for some limb-darkening laws, and Giménez (2006) shows how to compute $\alpha_{\mathrm{tra}}(t)$ for an arbitrary law based on earlier work by Kopal (1979).

By using one of these methods to calculate the flux of a limb-darkened disk with a circular obstruction, it is usually possible to model real transit light curves to within the measurement errors (see Section 4.3). In principle, calculations of occultation light curves should take the planetary limb darkening into account, though the precision of current data has not justified this level of detail. Likewise, in exceptional cases it may be necessary to allow for departures from circular shapes, due to rotational or tidal deformation (see Section 6). Modelers of eclipsing binary stars have long needed to take into account these and other subtle effects (Kallrath & Milone 2009, Hilditch 2001).

More generally, the loss of light depends on the intensity of the particular patch of the photosphere that is hidden by the planet. The planet provides a raster scan of the stellar intensity across the transit chord. In this manner, star spots and plages can be detected through the flux anomalies that are observed when the planet covers them. (An example is given in the top right panel of Figure 8.) Even spots that are not along the transit chord can produce observable effects, by causing variations in $F_\star$ and thereby causing $\delta_{\mathrm{tra}}$ to vary from transit to transit.

## 3. SCIENCE FROM ECLIPSES

### 3.1 Determining absolute dimensions

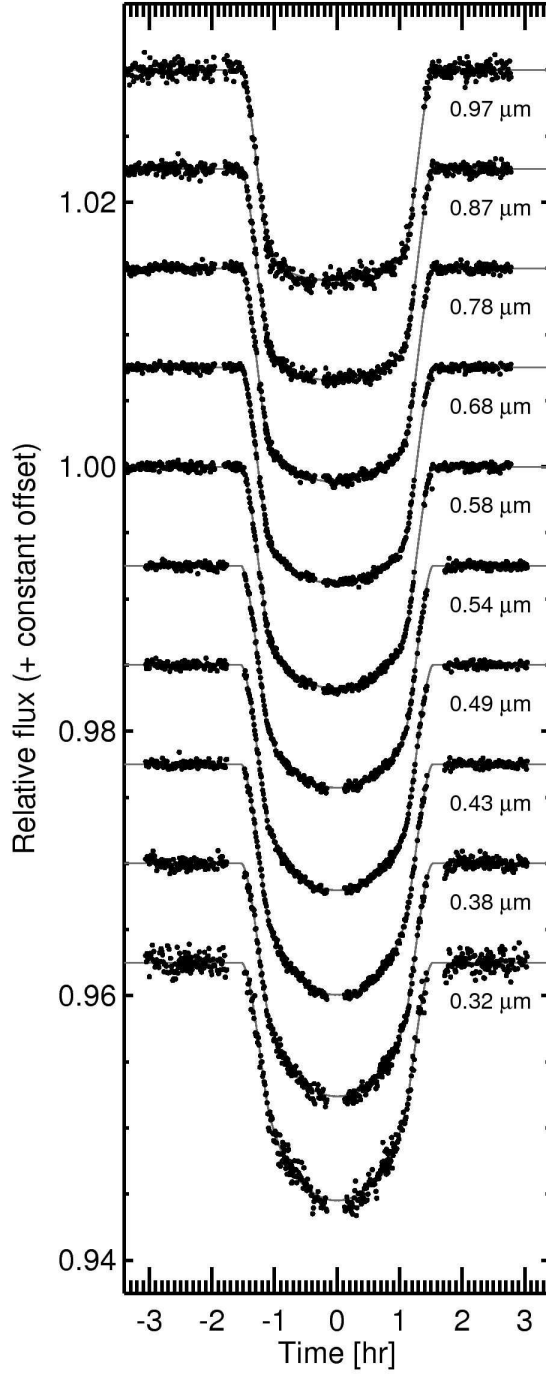Chief among the reasons to observe transits is to determine the mass and radius of the planet. Ideally one

Fig. 4.— Transits of the giant planet HD 209458b observed at wavelengths ranging from 0.32 $\mu$m (bottom) to 0.97 $\mu$m (top). At shorter wavelengths, the limb darkening of the star is more pronounced, and the bottom of the light curve is more rounded. The data were collected with the *Hubble Space Telescope* by Knutson et al. (2007a).

would like to know the mass in kilograms, and the radius in kilometers, to allow for physical modeling and comparisons with solar system planets. With only a transit light curve, this is impossible. The light curve by itself reveals the planet-to-star radius ratio $k \equiv R_p/R_\star \approx \sqrt{\delta}$ but not the planetary radius, and says nothing about the planetary mass.

To learn the planetary mass, in addition to the light curve one needs the radial-velocity orbit of the host star, and in particular the velocity semiamplitude $K_\star$. Using equation (66) of the chapter by Murray and Correia, and Kepler's third law, we may write

$$\frac{M_p}{(M_p + M_\star)^{2/3}} = \frac{K_\star\sqrt{1 - e^2}}{\sin i}\left(\frac{P}{2\pi G}\right)^{1/3}. \quad (25)$$

The observation of transits ensures $\sin i \approx 1$, and thereby breaks the usual $M_p \sin i$ degeneracy. However, the planetary mass still cannot be determined independently of the stellar mass. In the usual limit $M_p \ll M_\star$, the data determine $M_p/M_\star^{2/3}$ but not $M_p$ itself.

To determine the absolute dimensions of the planet, one must supplement the transit photometry and radial-velocity orbit with some external information about the star. Depending on the star, the available information may include its luminosity, spectral type, and spectrally-derived photospheric properties (effective temperature, surface gravity, and metallicity). A typical approach is to seek consistency between those data and stellar-evolutionary models, which relate the observable properties to the stellar mass, radius, composition, and age. In special cases it may also be possible to pin down the stellar properties using interferometry (Baines et al. 2009), asteroseismology (Stello et al. 2009), or an eclipsing companion star.

Besides $\delta$, the transit light curve offers the observables $T_{\rm tot}$ and $T_{\rm full}$ (or $T$ and $\tau$), which can be used to solve for the impact parameter $b$ and the *scaled stellar radius $R_\star/a$*. For non-grazing transits, in the limit $R_p \ll R_\star \ll a$ we may invert equations (14-15) to obtain the approximate formulas

$$b^2 = \frac{(1 - \sqrt{\delta})^2 - (T_{\rm full}/T_{\rm tot})^2(1 + \sqrt{\delta})^2}{1 - (T_{\rm full}/T_{\rm tot})^2} \quad (26)$$

$$\frac{R_\star}{a} = \frac{\pi}{2\delta^{1/4}}\frac{\sqrt{T_{\rm tot}^2 - T_{\rm full}^2}}{P}\left(\frac{1 + e\sin\omega}{\sqrt{1 - e^2}}\right). \quad (27)$$

If in addition $\tau \ll T$, such as is the case for small planets on non-grazing trajectories, the results are simplified still further to

$$b^2 = 1 - \sqrt{\delta}\frac{T}{\tau}, \quad (28)$$

$$\frac{R_\star}{a} = \frac{\pi}{\delta^{1/4}}\frac{\sqrt{T\tau}}{P}\left(\frac{1 + e\sin\omega}{\sqrt{1 - e^2}}\right). \quad (29)$$

The orbital inclination $i$ may then be obtained using equation (7). These approximations are useful for theoretical calculations and for developing an intuition about how the

system parameters affect the observable light curve. For example, $R_\star/a$ controls the product of $T$ and $\tau$ while $b$ controls their ratio. However, as mentioned earlier, for fitting actual data one needs a realistic limb-darkened model, linked to a Keplerian orbital model.

The dimensionless ratios $R_\star/a$ and $R_p/a$ are important for several reasons: (i) They set the scale of tidal interactions between the star and planet. (ii) $R_p/a$ determines what fraction of the stellar luminosity impinges on the planet, as discussed in Section 3.4. (iii) $R_\star/a$ can be used to determine a particular combination of the stellar mean density $\rho_\star$ and planetary mean density $\rho_p$:

$$\rho_\star + k^3 \rho_p = \frac{3\pi}{GP^2}\left(\frac{a}{R_\star}\right)^3. \tag{30}$$

This can be derived from Kepler's third law (Seager & Mallen-Ornelas 2003). Since $k^3$ is usually small, the second term on the left side of equation (30) is often negligible and $\rho_\star$ can be determined purely from transit photometry.

This method for estimating $\rho_\star$ has proven to be a useful diagnostic in photometric transit surveys: a true transit signal should yield a value of $\rho_\star$ that is consistent with expectations for a star of the given luminosity and spectral type. Furthermore, once a precise light curve is available, $\rho_\star$ is a valuable additional constraint on the stellar properties.

Interestingly, it is possible to derive the planetary surface gravity $g_p \equiv GM_p/R_p^2$ independently of the stellar properties:

$$g_p = \frac{2\pi}{P}\frac{\sqrt{1-e^2}\,K_\star}{(R_p/a)^2 \sin i}. \tag{31}$$

This is derived from equation (66) of the chapter by Murray and Correia and Kepler's third law (Southworth et al. 2007).

In short, precise transit photometry and Doppler velocimetry lead to correspondingly precise values of the stellar mean density $\rho_\star$ and planetary surface gravity $g_p$. However, the errors in $M_p$ and $R_p$ are ultimately limited by the uncertainties in the stellar properties.

### 3.2 Timing of eclipses

The orbital period $P$ can be determined by timing a sequence of transits, or a sequence of occultations, and fitting a linear function

$$t_c[n] = t_c[0] + nP, \tag{32}$$

where $t_c[n]$ is the time of conjunction of the $n$th event. The times must first be corrected to account for the Earth's orbital motion and consequent variations in the light travel time. When comparing transit and occultation times, one must further correct for the light travel time across the line-of-sight dimension of the planetary orbit. As long as there is no ambiguity in $n$, the error in $P$ varies inversely as the total number of eclipses spanned by the observations, making it possible to achieve extraordinary precision in $P$.

If the orbit does not follow a fixed ellipse—due to forces from additional bodies, tidal or rotational bulges, general

relativity, or other non-Keplerian effects—then there will be variations in the interval between successive transits, as well as the interval between transits and occultations and the shape of the transit light curve. These variations may be gradual parameter changes due to precession (Miralda-Escudé 2002), or short-term variations due to other planets (Holman & Murray 2005, Agol et al. 2005) or moons (Kipping 2009). The effects can be especially large for bodies in resonant orbits with the transiting planet. By monitoring transits one might hope to detect such bodies, as discussed in the chapter by Fabrycky.

When transits and occultations are both seen, a powerful constraint on the shape of the orbit is available. For a circular orbit, those events are separated in time by $P/2$, but more generally the time interval depends on $e$ and $\omega$. To first order in $e$, integrating $dt/df$ between conjunctions gives

$$\Delta t_c \approx \frac{P}{2}\left[1 + \frac{4}{\pi}e\cos\omega\right]. \tag{33}$$

In this case, the timing of transits and occultations gives an estimate of $e\cos\omega$. Likewise the relative durations of the transit and the occultation depend on the complementary parameter $e\sin\omega$,

$$\frac{T_{\rm occ}}{T_{\rm tra}} \approx \frac{1 + e\sin\omega}{1 - e\sin\omega}. \tag{34}$$

Sterne (1940) and de Kort (1954) give the lengthy exact results for arbitrary $e$ and $i$. Because the uncertainty in $\Delta t_c/P$ is typically smaller than that in $T_{\rm tra}/T_{\rm occ}$ (by a factor of $P/T$), the eclipse data constrain $e\cos\omega$ more powerfully than $e\sin\omega$.

The resulting bounds on $e$ are often valuable. For example, planets on close-in eccentric orbits are internally heated by the friction that accompanies the time-variable tidal distortion of the planet. Empirical constraints on $e$ thereby help to understand the thermal structure of close-in planets. For more distant planets, bounds on $e$ are helpful in the statistical analysis of exoplanetary orbits. As described in the chapter by Cumming and in Part V of this volume, the observed eccentricity distribution of planetary orbits is a clue about the processes of planet formation and subsequent orbital evolution.

Eclipse-based measurements of $t_{\rm tra}$, $t_{\rm occ}$, and $P$ are almost always more precise than those based on spectroscopic or astrometric orbital data. The eclipse-based results can greatly enhance the analysis of those other data. For example, the usual radial-velocity curve has 6 parameters, but if $t_{\rm tra}$, $t_{\rm occ}$, and $P$ are known from eclipses, the number of free parameters is effectively reduced to 3, thereby boosting the achievable precision in the other 3 parameters.

### 3.3 Transmission spectroscopy

We have been implicitly assuming that the planetary silhouette has a sharp edge, but in reality the edge is fuzzy. For gas giant planets there is no well-defined surface, and even

planets with solid surfaces may have thick atmospheres. During a transit, a small portion of the starlight will be filtered through the upper atmosphere of the planet, where it is only partially absorbed. The absorption will be wavelength-dependent due to the scattering properties of atoms and molecules in the planetary atmosphere. At the wavelength of a strong atomic or molecular transition, the atmosphere is more opaque, and the planet's effective silhouette is larger. This raises the prospect of measuring the *transmission spectrum* of the planet's upper atmosphere and thereby gaining knowledge of its composition.

To calculate the expected signal one must follow the radiative transfer of the incident starlight along a grazing trajectory through the planet's stratified atmosphere. The calculation is rather complicated (see, e.g., Seager & Sasselov 2000, Brown 2001) but the order of magnitude of the effect is easily appreciated. For a strong transition, the effective size of the planet grows by a few atmospheric scale heights $H$, where

$$H = \frac{k_B T}{\mu_m g} \qquad (35)$$

and $T$ is the temperature, $\mu_m$ is the mean molecular mass, $g$ is the local gravitational acceleration, and $k_B$ is Boltzmann's constant. Defining $R_p$ as the radius within which the planet is optically thick at all wavelengths, the extra absorption due to the optically thin portion of the atmosphere causes the transit depth to increase by

$$\Delta\delta = \frac{\pi(R_p + N_H H)^2}{\pi R_\star^2} - \frac{\pi R_p^2}{\pi R_\star^2} \approx 2N_H \delta \left(\frac{H}{R_p}\right), \quad (36)$$

where $N_H$, the number of scale heights, is of order unity. The signal is most readily detectable for planets with large $H$: low surface gravity, low mean molecular mass, and high temperature. For a "hot Jupiter" around a Sun-like star ($\delta = 0.01$, $T \approx 1300$ K, $g \approx 25$ m s$^{-2}$, $\mu_m = 2$ amu) the signal is $\Delta\delta \sim 10^{-4}$. For an Earth-like planet around a Sun-like star ($\delta = 10^{-4}$, $T \approx 273$ K, $g \approx 10$ m s$^{-2}$, $\mu_m = 28$ amu), the signal is $\Delta\delta \sim 10^{-6}$.

The signal can be detected by observing a transit light curve at multiple wavelengths, using different filters or a spectrograph. One then fits a limb-darkened light-curve model to the time series obtained at each wavelength, requiring agreement in the orbital parameters and allowing a value of $\delta$ specific to each wavelength. The resulting variations in $\delta(\lambda)$ are expected to be of the order of magnitude given by equation (36). It is best to gather all of the data at the same time, because intrinsic stellar variability is also chromatic.

### 3.4 Occultation spectroscopy

As discussed in Section 2.4, when the planet is completely hidden the starlight declines by a fraction $\delta_{\rm occ} = k^2 I_p/I_\star$, where $k$ is the planet-to-star radius ratio and $I_p/I_\star$ is the ratio of disk-averaged intensities. Observations spanning occultations thereby reveal the relative brightness of the planetary disk, if $k$ is already known from transit observations. The planetary radiation arises from two sources: thermal radiation and reflected starlight. Because the planet is colder than the star, the thermal component emerges at longer wavelengths than the reflected component.

For the moment we suppose that the planet is of uniform brightness, and that the observing wavelength is long enough for thermal emission to dominate. Approximating the planet and star as blackbody radiators,

$$\delta_{\rm occ}(\lambda) = k^2 \frac{B_\lambda(T_p)}{B_\lambda(T_\star)} \longrightarrow k^2 \frac{T_p}{T_\star} \qquad (37)$$

where $B_\lambda(T)$ is the Planck function,

$$B_\lambda(T) \equiv \frac{2hc^2}{\lambda^5} \frac{1}{e^{hc/(\lambda k_B T)} - 1} \longrightarrow \frac{2ck_B T}{\lambda^4}, \qquad (38)$$

in which $T$ is the temperature, $\lambda$ is the wavelength, $h$ is Planck's constant, and $c$ is the speed of light. The limiting cases are for the "Rayleigh-Jeans" limit $\lambda \gg hc/(k_B T)$. The decrement $\delta_{\rm occ}$ that is observed by a given instrument is obtained by integrating equation (37) over the bandpass.

Even when the planetary radiation is not described by the Planck law, one may define a *brightness temperature* $T_b(\lambda)$ as the equivalent blackbody temperature that would lead to the observed value of $\delta_{\rm occ}(\lambda)$. The brightness temperature is sometimes a convenient way to describe the wavelength-dependent intensity even when it is not thermal in origin.

There may be departures from a blackbody spectrum—spectral features—discernible in the variation of brightness temperature with wavelength. In contrast with transmission spectroscopy, which refers to starlight that grazes the planetary limb (terminator), here we are referring to the emission spectrum of the planet averaged over the visible disk of the dayside. Occultation spectroscopy and transit spectroscopy thereby provide different and complementary information about the planetary atmosphere.

It is possible to measure the reflectance spectrum of the planet's dayside by observing at shorter wavelengths, or accurately subtracting the thermal emission. The occultation depth due to reflected light alone is

$$\delta_{\rm occ}(\lambda) = A_\lambda \left(\frac{R_p}{a}\right)^2, \qquad (39)$$

where $A_\lambda$ is the *geometric albedo*, defined as the flux reflected by the planet when viewed at opposition (full phase), divided by the flux that would be reflected by a flat and perfectly diffusing surface with the same cross-sectional area as the planet. One of the greatest uncertainties in atmospheric modeling is the existence, prevalence, and composition of clouds. Since clouds can produce very large albedo variations, reflectance spectroscopy may help to understand the role of clouds in exoplanetary atmospheres.

For a close-in giant planet, the reflectance signal is $\sim 10^{-4}$ while for an Earthlike planet at 1 AU it is $\sim 10^{-9}$. The detection prospects are better for closer-in planets.

However, the closest-in planets are also the hottest, and their radiation may be dominated by thermal emission. Another consideration is that planets with $T > 1500$ K are expected to be so hot that all potentially cloud-forming condensable materials are in gaseous form. The theoretically predicted albedos are very low, of order $10^{-3}$, due to strong absorption by neutral sodium and potassium.

Real planets do not have uniformly bright disks. Gaseous planets are limb darkened or brightened, and may have latitudinal zones with high contrast, like Jupiter. Rocky planets may have surface features and oceans. To the extent that departures from uniform brightness could be detected, occultation data would provide information on the spatially-resolved planetary dayside. Specifically, the light curve of the ingress or egress of an occultation gives a one-dimensional cumulative brightness distribution of the planet.

### 3.5 The Rossiter-McLaughlin effect

In addition to the spectral variations induced by the planetary atmosphere, there are spectral variations arising from the spatial variation of the stellar spectrum across the stellar disk. The most pronounced of these effects is due to stellar rotation: light from the approaching half of the stellar disk is blueshifted, and light from the receding half is redshifted. Outside of transits, rotation broadens the spectral lines but does not produce an overall Doppler shift in the disk-integrated starlight. However, when the planet covers part of the blueshifted half of the stellar disk, the integrated starlight appears slightly redshifted, and vice versa.

Thus, the transit produces a time-variable spectral distortion that is usually manifested as an "anomalous" radial velocity, i.e., a Doppler shift that is greater or smaller than the shift expected from only the star's orbital motion. Figure 5 illustrates this effect. It is known as the Rossiter-McLaughlin (RM) effect, after the two astronomers who made the first definitive observations of this kind for binary stars, in 1924.

The maximum amplitude of the anomalous radial velocity is approximately

$$\Delta V_{\mathrm{RM}} \approx k^2 \sqrt{1 - b^2} (v_\star \sin i_\star), \qquad (40)$$

where $v_\star \sin i_\star$ is the line-of-sight component of the stellar equatorial rotation velocity. For a Sun-like star ($v_\star \sin i_\star = 2$ km s$^{-1}$), the maximum amplitude is $\sim$20 m s$^{-1}$ for a Jovian planet and $\sim$0.2 m s$^{-1}$ for a terrestrial planet. This amplitude may be comparable to (or even larger than) the amplitude of the spectroscopic orbit of the host star. Furthermore it is easier to maintain the stability of a spectrograph over the single night of a transit than the longer duration of the orbital period. Hence the RM effect is an effective means of detecting and confirming transits, providing an alternative to photometric detection.

In addition, by monitoring the anomalous Doppler shift throughout a transit, it is possible to measure the angle on the sky between the planetary orbital axis and the stellar rotation axis. Figure 6 shows three trajectories of a transiting planet that have the same impact parameter, and hence produce identical light curves, but that have different orientations relative to the stellar spin axis, and hence produce different RM signals. The signal for a well-aligned planet is antisymmetric about the midtransit time (left panels), whereas a strongly misaligned planet that blocks only the receding half of the star will produce only an anomalous blueshift (right panels).

A limitation of this technique is that it is only sensitive to the angle between the *sky projections* of the spin and orbital angular momentum vectors. The true angle between those vectors is usually poorly constrained because $i_\star$ is unknown. Nevertheless it may be possible to tell whether the planetary orbit is prograde or retrograde, with respect to the direction of stellar rotation. It is also possible to combine results from different systems to gain statistical knowledge about spin-orbit alignment.

More broadly, just as transit photometry provides a raster scan of the intensity of the stellar photosphere along the transit chord, RM data provide a raster scan of the line-of-sight velocity field of the photosphere. This gives an independent measure of the projected rotation rate $v_\star \sin i_\star$, and reveals the velocity structure of starspots or other features that may exist on the photosphere.

### 4. OBSERVING ECLIPSES

### 4.1 Discovering eclipsing systems

Figure 7 shows the rate of exoplanet discoveries over the last 20 years, highlighting the subset of planets known to transit. Transits have been discovered in two ways. One way is to find the planet in a Doppler survey (see chapter by Lovis and Fischer), and then check for transits by monitoring the brightness of the star throughout the inferior conjunction. This was the path to discovery for 6 of the 64 known systems, including the first example, HD 209458b (Charbonneau et al. 2000, Henry et al. 2000, Mazeh et al. 2000). The probability that transits will occur is given by equation (9) and the times of inferior conjunction can be calculated from the parameters of the spectroscopic orbit (Kane 2007).

The other way is to conduct photometric surveillance of stars that are not yet known to have any planets, an idea dating back to Struve (1952). As an illustration let us consider the requirements for a program to discover hot Jupiters. As discussed in Section 2.2, a bare minimum of $10^3$ Sun-like stars must be examined to find a transiting planet with an orbital distance of 0.05 AU. The observations must be precise enough to detect a 1% flux drop, and must extend for at least several times longer than the 3 day orbital period. The difficulty increases dramatically for smaller planets in wider orbits: in an idealized survey of nearby field stars limited by photon noise (see Section 4.2) the sensitivity to
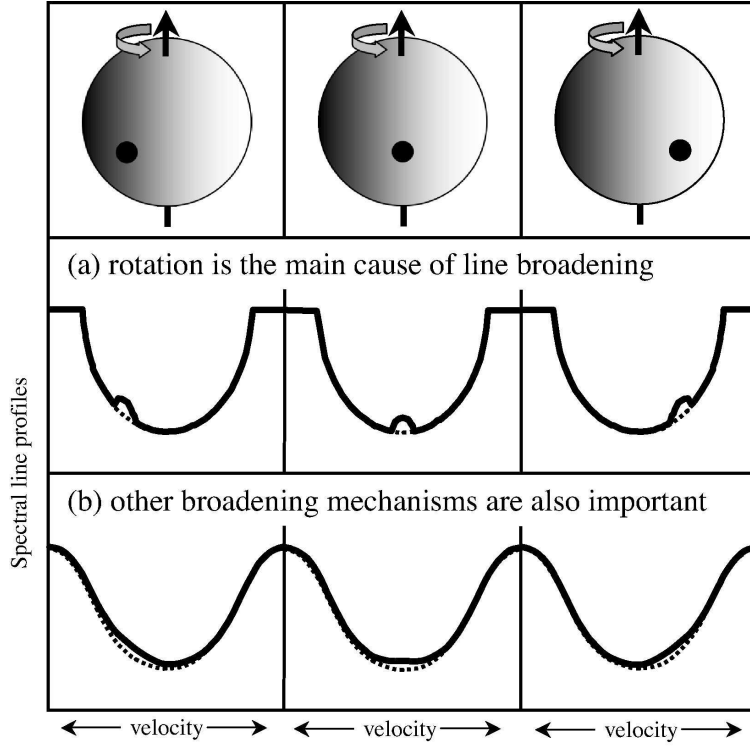
Fig. 5.— Illustration of the Rossiter-McLaughlin (RM) effect. The three columns show three successive phases of a transit. The first row shows the stellar disk, with the grayscale representing the projected rotation velocity: the approaching limb is black and the receding limb is white. The second row shows the corresponding stellar absorption line profiles, assuming rotation to be the dominant broadening mechanism. The "bump" occurs because the planet hides a fraction of the light that contributes a particular velocity to the line-broadening kernel. The third row shows the case for which other line-broadening mechanisms are important; here the RM effect is manifested only as an "anomalous Doppler shift." Adapted from Gaudi & Winn (2007).
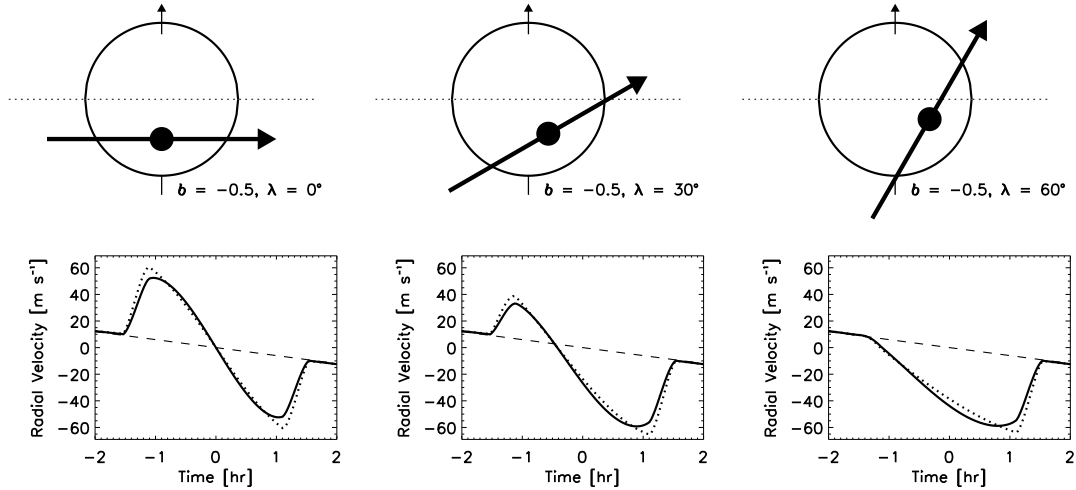


Fig. 6.— Using the RM effect to measure the angle $\lambda$ between the sky projections of the orbital and stellar-rotational axes. Three different possible trajectories of a transiting planet are shown, along with the corresponding RM signal. The trajectories all have the same impact parameter and produce the same light curve, but they differ in $\lambda$ and produce different RM curves. The dotted lines are for the case of no limb darkening, and the solid lines include limb darkening. From Gaudi & Winn (2007).
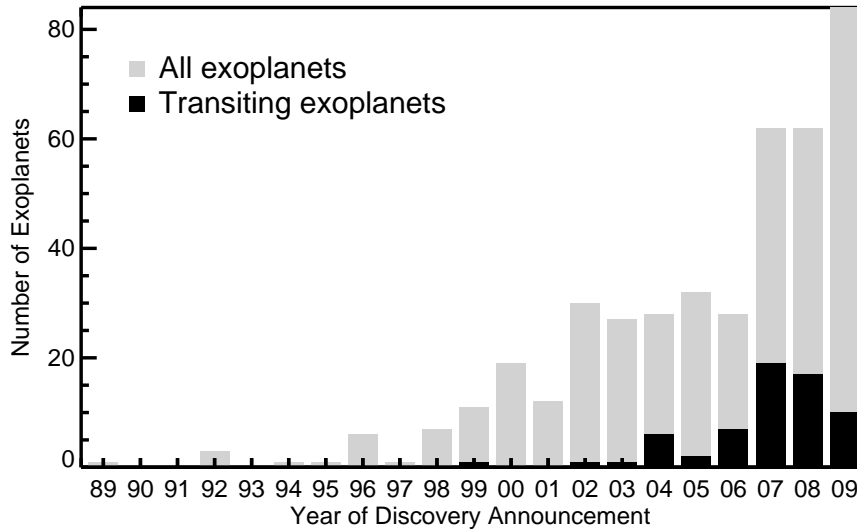
10

Fig. 7.— Rate of exoplanet discovery. The light bars show the number of announcements of newly discovered planets, and the dark bars show the subset of transiting planets. Compiled with data from exoplanet.eu, an encyclopedic web site maintained by J. Schneider.

transiting planets scales approximately as $R_p^6/P^{5/3}$ (Gaudi 2005; Gaudi, Seager, & Mallen-Ornelas 2005). More realistic calculations take into account the spread in radius and luminosity among the surveyed stars, the duration and time-sampling of observations, the appropriate threshold value of the signal-to-noise ratio, and other factors (see, e.g., Pepper et al. 2003, Beatty & Gaudi 2008).

Photometric surveys are much less efficient than Doppler surveys, in the sense that only a small fraction of planets transit, and even when transits occur they are underway only a small fraction of the time. On the other hand, the starting equipment for a photometric survey is modest, consisting in some cases of amateur-grade telescopes or telephoto lenses and cameras, whereas Doppler surveys require upfront a large telescope and sophisticated spectrograph. For these reasons the royal road of eclipses enticed many astronomers to embark on photometric transit surveys. More than a dozen surveys were undertaken, including a few longitudinally-distributed networks to provide more continuous time coverage. Major efforts were made to automate the observations, and to develop algorithms for precise wide-field photometry (Tamuz et al. 2005, Kovács et al. 2005) and transit detection (Kovács et al. 2002). Horne (2003) took stock of all the ongoing and planned surveys, and ventured to predict a bounty of 10–100 new planets per month, in an article subtitled "Hot Jupiters Galore."

The royal road turned out to have some potholes. One obstacle was the high rate of "false positives," signals that resemble planetary transits but are actually grazing eclipses of a binary star, or an unresolved combination of an eclipsing binary star and a third star. In the latter case, the deep eclipses of the binary star are diluted to planet-like proportions by the constant light of the third star. In some surveys

the false positives outnumbered the planets by 10 to 1. Ruling them out required spectroscopy with large telescopes, which became the bottleneck in the discovery process (see, e.g., O'Donovan et al. 2007). Another obstacle was correlated noise ("red noise") in the survey photometry (see Section 4.3). Pont et al. (2006) showed that red noise slashed the sensitivity of the search algorithms, thereby providing a quantitative solution to the "Horne problem" of why transiting planets were not being found as rapidly as expected.

Only a few of the surveyors were able to overcome these obstacles. The 5 most successful surveys were OGLE, which used a 1 m telescope to survey 14-16th magnitude stars; and the TrES, XO, HAT, and SuperWASP surveys, which used ≈0.1 m lenses to survey 10-12th magnitude stars. Many of today's transiting planets are named after these surveys: for more details see Udalski et al. (2002), Alonso et al. (2004), McCullough et al. (2005), Bakos et al. (2007), and Pollacco et al. (2006). The OGLE planets were found first, although the brighter stars from the wider-field surveys were far more amenable to false-positive rejection and detailed characterization.

On the other end of the cost spectrum are photometric surveys performed from space. By avoiding the deleterious effects of the Earth's atmosphere, it is possible to beat the precision of ground-based observations (see Section 4.2). It is also possible to avoid the usual interruptions due to the vagaries of the weather, and even to avoid the day-night cycle if the spacecraft is in an orbit far from Earth. The two ongoing space-based missions *CoRoT* and *Kepler* are described in Sections 5.1 and 6, respectively.

One space-based survey that did not discover any planets nevertheless produced an interesting result. Gilliland et al. (2000) used the *Hubble Space Telescope* to seek close-in giant planets in the globular cluster 47 Tucanae. No transits

were found, even though 17 were expected based on the survey characteristics and the observed frequency of close-in giant planets around nearby field stars. The absence of close-in planets could be due to the crowded stellar environment (which could inhibit planet formation or disrupt planetary systems) or the cluster's low metallicity (which has been found to be correlated with fewer planets in the Doppler surveys; see the chapters by Lovis and Fischer and by Cumming). The null results of a subsequent survey of the less-crowded outskirts of 47 Tucanae suggest that crowding is not the primary issue (Weldrake et al. 2005).

### 4.2 Measuring the photometric signal

Even after a transiting planet is discovered, it takes a careful hand to measure the transit signal precisely enough to achieve the scientific goals set forth in Section 3. The loss of light is only 1% for a Sun-like star crossed by a Jupiter-sized planet, and 0.01% for an Earth-sized planet. Occultations produce still smaller signals. This is the domain of precise time-series differential photometry. The term "differential" applies because only the fractional variations are of interest, as opposed to the actual intensity in Janskys or other standardized units. Eclipses can also be detected via spectroscopy (Section 3.5) or polarimetry (Carciofi & Magalhães 2005) but here we focus on the photometric signal, with emphasis on ground-based optical observations.

First you must know when to observe. To observe an eclipse requires a triple coincidence: the eclipse must be happening, the star must be above the horizon, and the Sun must be down. Transit times can be predicted based on a sequence of previously measured transit times, by fitting and extrapolating a straight line (equation 32). Occultation times can also be predicted from a listing of transit times, but are subject to additional uncertainty due to the dependence on $e$ and $\omega$ (equation 33).

Next you should monitor the flux of the target star along with other nearby stars of comparable brightness. The measured fluxes are affected by short-term variations in atmospheric transparency, as well as the gradual change in the effective atmospheric path length (the *airmass*) as the star rises and sets. However, the ratios of the fluxes between nearby stars are less affected. As long as some of the comparison stars are constant in brightness then the relative flux of the target star can be tracked precisely.

This task is usually accomplished with a charge-coupled device (CCD) imaging camera and software for calibrating the images, estimating the sky background level, and counting the photons received from each star in excess of the sky level (*aperture photometry*). Howell (1999) explains the basic principles of CCDs and aperture photometry. For more details on differential aperture photometry using an ensemble of comparison stars, see Gilliland & Brown (1988), Kjeldsen & Frandsen (1992), and Everett & Howell (2001). In short, the fluxes of the comparison stars are combined, and the flux of the target star is divided by the comparison signal, giving a time series of relative flux

measurements spanning the eclipse with as little noise as possible. For bright stars observed at optical wavelengths, among the important noise sources are photon noise, scintillation noise, differential extinction, and flat-fielding errors, which we now discuss in turn.

*Photon noise* refers to the unavoidable fluctuations in the signal due to the quantization of light. It is also called *Poisson noise* because the photon count rate obeys a Poisson distribution. If a star delivers $N$ photons s$^{-1}$ on average, then the standard deviation in the relative flux due to photon noise is approximately $(N\Delta t)^{-1/2}$ for an exposure lasting $\Delta t$ seconds. This noise source affects the target and comparison stars independently. The sky background also introduces Poisson noise, which can be troublesome for faint stars or infrared wavelengths. The photon noise in the comparison signal can be reduced by using many bright comparison stars. Beyond that, improvement is possible only by collecting more photons, using a bigger telescope, a more efficient detector, or a wider bandpass.

*Scintillation* is caused by fluctuations in the index of refraction of air. The more familiar term is "twinkling." For integration times $\Delta t \gtrsim 1$ s, the standard deviation in the relative flux due to scintillation is expected to scale with telescope diameter $D$, observatory altitude $h$, integration time, and airmass as

$$\sigma_{\rm scin} = \sigma_0 \frac{({\rm Airmass})^{7/4}}{D^{2/3}(\Delta t)^{1/2}} \exp\left(-\frac{h}{8000\,{\rm m}}\right), \qquad (41)$$

based on a theory of atmospheric turbulence by Reiger (1963), with empirical support from Young (1967) and others. The coefficient $\sigma_0$ is often taken to be 0.064 when $D$ is expressed in centimeters and $\Delta t$ in seconds, but this must be understood to be approximate and dependent on the local meteorology. Scintillation affects both the target and comparison stars, although for closely-spaced stars the variations are correlated (Ryan & Sandler 1998). One also expects scintillation noise to decrease with wavelength. Thus, scintillation noise is reduced by employing a large telescope (or combining results from multiple small telescopes), choosing nearby comparison stars, and observing at a long wavelength from a good site.

*Differential extinction* is used here as a shorthand for "second-order color-dependent differential extinction." To first order, if two stars are observed simultaneously, their fluxes are attenuated by the Earth's atmosphere by the same factor and the flux ratio is preserved. To second order, the bluer star is attenuated more, because scattering and absorption are more important at shorter wavelengths. This effect causes the flux ratio to vary with airmass as well as with short-term transparency fluctuations. It can be reduced by choosing comparison stars bracketing the target star in color, or using a narrow bandpass. The advantage of a narrow bandpass must be weighed against the increased photon noise.

*Flat fielding* is the attempt to correct for nonuniform illumination of the detector and pixel-to-pixel sensitivity variations, usually by dividing the images by a calibration image

of a uniformly-lit field. If the stars were kept on the same pixels throughout an observation, then flat-fielding errors would not affect the flux ratios. In reality the light from a given star is detected on different pixels at different times, due to pointing errors, focus variations, and seeing variations. Imperfect flat fielding coupled with these variations produce noise in the light curve. The impact of flat-fielding errors is reduced by ensuring the calibration images have negligible photon noise, maintaining a consistent pointing, and defocusing the telescope. Defocusing averages down the interpixel variations, reduces the impact of seeing variations, and allows for longer exposure times without saturation, thereby increasing the fraction of the time spent collecting photons as opposed to resetting the detector. Defocusing is good for what ails you, as long as the stars do not blend together.

This discussion of noise sources is not exhaustive; it is in the nature of noise that no such listing can be complete. For example, the gain of the detector may drift with temperature, or scattered moonlight may complicate background subtraction. A general principle is to strive to keep everything about the equipment and the images as consistent as possible. Another good practice is to spend at least as much time observing the star before and after the eclipse as during the eclipse, to establish the baseline signal and to characterize the noise.

It is often advisable to use a long-wavelength bandpass, not only to minimize scintillation and differential extinction, but also to reduce the effects of stellar limb darkening on the transit light curve. The degree of limb darkening diminishes with wavelength because the ratio between blackbody spectra of different temperatures is a decreasing function of wavelength. Transit light curves observed at longer wavelengths are "boxier," with sharper corners and flatter bottoms. All other things being equal, this reduces the statistical uncertainties in the transit parameters, but other factors should also be considered. For example, at infrared wavelengths, limb darkening may be small, but the sky background is bright and variable.

The space-based observer need not worry about scintillation and differential extinction, and enjoys a low background level even at infrared wavelengths. Extremely precise photometry is possible, limited only by the size of the telescope and the degree to which the detector is well-calibrated. With the *Hubble Space Telescope* a precision of approximately $10^{-4}$ per minute-long integration has been achieved, a few times better than the best ground-based light curves. Figure 8 allows for some side-by-side comparisons of ground-based and space-based data. However, going to space is not a panacea. When unforeseen calibration issues arise after launch, they are difficult to resolve. In low Earth orbit, there are also unhelpful interruptions due to occultations by the Earth, as well as problems with scattered Earthshine and cosmic rays. More remote orbits offer superior observing conditions, but require greater effort and expense to reach.
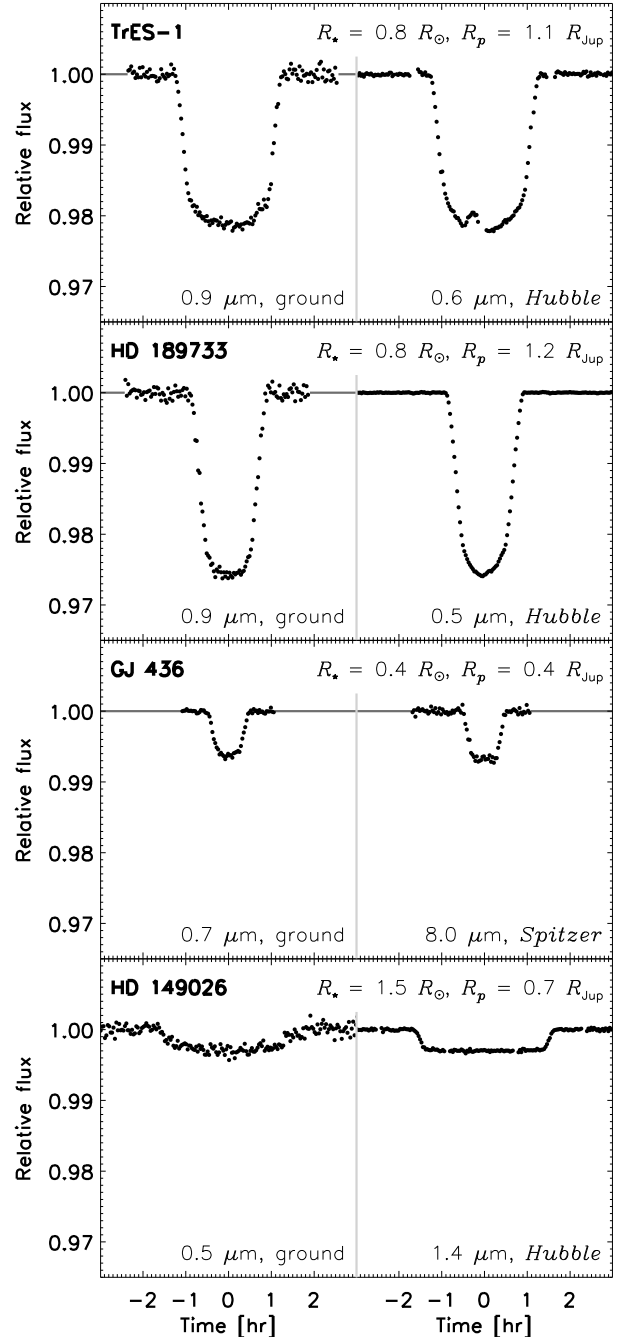


Fig. 8.— Examples of transit light curves based on ground-based observations (left) and space-based observations (right). In the top right panel, the "bump" observed just before midtransit is interpreted as the covering of a dark starspot by the planet. From upper left to lower right, the references are Winn et al. (2007a), Rabus et al. (2009), Winn et al. (2007b), Pont et al. (2008), Holman et al. in prep., Gillon et al. (2007), Winn et al. (2008), and Carter et al. (2009).

## 4.3 Interpreting the photometric signal

Once you have an eclipse light curve, the task remains to derive the basic parameters $\{\delta, T, \tau, t_c\}$ and their uncertainties, as well as the results for other quantities such as $g_p$ and $\rho_\star$ that can be derived from those parameters. The analytic equations given in Section 2 for the eclipse duration, timing, and other properties are rarely used to analyze data. Rather, a parametric model is fitted to the data, based on the numerical integration of Kepler's equation to calculate the relative positions of the star and planet, as well as one of the prescriptions mentioned in Section 2.4 for computing the loss of light from the limb-darkened stellar photosphere.

The first task is writing a code that calculates the light curve of the star-planet system as a function of the orbital parameters and eclipse parameters. Then, this code is used in conjunction with one of many standard routines to optimize the parameter values, typically by minimizing the sum-of-squares statistic,

$$\chi^2 = \sum_{i=1}^{N} \left[ \frac{f_i(\text{obs}) - f_i(\text{calc})}{\sigma_i} \right]^2, \qquad (42)$$

where $f_i(\text{obs})$ is the observed value of relative flux at time $t_i$, $f_i(\text{calc})$ is the calculated flux (depending on the model parameters), and $\sigma_i$ is the measurement uncertainty. The techniques found in standard works such as Numerical Recipes (Press et al. 2007) are applicable here, although a few points of elaboration are warranted for the specific context of eclipse photometry.

It is common to adopt a Bayesian attitude, in which the parameters are viewed as random variables whose probability distributions ("posteriors") are constrained by the data. This can be done in a convenient and elegant fashion using the Monte Carlo Markov Chain (MCMC) method, in which a chain of points is created in parameter space using a few simple rules that ensure the collection of points will converge toward the desired posterior. This method gives the full multidimensional joint probability distribution for all the parameters, rather than merely giving individual error bars, making it easy to visualize any fitting degeneracies and to compute posteriors for any combination of parameters that may be of interest. Although a complete MCMC briefing is beyond the scope of this chapter, the interested reader should consult the textbook by Gregory (2005) as well as case studies such as Holman et al. (2006), Collier Cameron et al. (2007), and Burke et al. (2007).

A vexing problem is the presence of correlated noise, as mentioned in Section 4.2. The use of equation (42) is based on the premise that the measurement errors are statistically independent. In many cases this is plainly false. Real light curves have bumps, wiggles, and slopes spanning many data points. These can be attributed to differential extinction, flat-fielding errors, or astrophysical effects such as starspots. Thus the number of truly independent samples is smaller than the number of data points, and the power to constrain model parameters is correspondingly reduced. Ignoring the correlations leads to false precision in the derived parameters, but accounting for correlations is not straightforward and can be computationally intensive. Some suggestions are given by Pont et al. (2006) and Carter & Winn (2009a).

The treatment of stellar limb darkening presents another unwelcome opportunity to underestimate the parameter uncertainties. It is tempting to adopt one of the standard limb-darkening laws (see Section 2.5) and hold the coefficients fixed at values deemed appropriate for the host star, based on stellar-atmosphere models. However, with precise data it is preferable to fit for the coefficients, or at least to allow for some uncertainty in the atmospheric models. In those few cases where the data have been precise enough to test the models, the models have missed the mark (Claret 2009).

Although fitting data is a job for a computer, it is nevertheless useful to have analytic formulas for the achievable precision in the eclipse parameters. The formulas are handy for planning observations, and for order-of-magnitude estimates of the observability (or not) of effects such as variations in transit times and durations. The formulas given here are based on the assumptions that the data have uniform time sampling $\Delta t$, and independent Gaussian errors $\sigma$ in the relative flux. A useful figure of merit is $Q \equiv \sqrt{N}\delta/\sigma$, where $\delta$ is the transit depth and $N$ is the number of data points obtained during the transit. A Fisher information analysis (essentially a glorified error propagation) leads to estimates for the $1\sigma$ uncertainties in the transit parameters (Carter et al. 2008):

$$\sigma_\delta \;\approx\; Q^{-1}\delta, \qquad (43)$$
$$\sigma_{t_c} \;\approx\; Q^{-1}T\sqrt{\tau/2T}, \qquad (44)$$
$$\sigma_T \;\approx\; Q^{-1}T\sqrt{2\tau/T}, \qquad (45)$$
$$\sigma_\tau \;\approx\; Q^{-1}T\sqrt{6\tau/T}, \qquad (46)$$

which are valid when $\delta \ll 1$, limb darkening is weak, and the out-of-transit flux is known precisely. In this case, $\sigma_{t_c} < \sigma_T < \sigma_\tau$. Correlated errors and limb darkening cause these formulas to be underestimates.

## 5. SUMMARY OF RECENT ACHIEVEMENTS

### 5.1 Discoveries of transiting planets

Discoveries of exoplanets, and transiting exoplanets in particular, have abounded in recent years (Figure 7). As of December 2009, approximately 64 transiting planets are known, representing 15% of the total number of exoplanets discovered. Figure 9 shows their masses, radii, and orbital periods. It is important to remember that these planets are *not* a randomly selected subset of exoplanets. The properties of the ensemble have been shaped by powerful selection effects in the surveys that led to their discovery, favoring large planets in short-period orbits.

Despite these selection effects, the known transiting planets exhibit a striking diversity. They span three orders of magnitude in mass, and one order of magnitude in
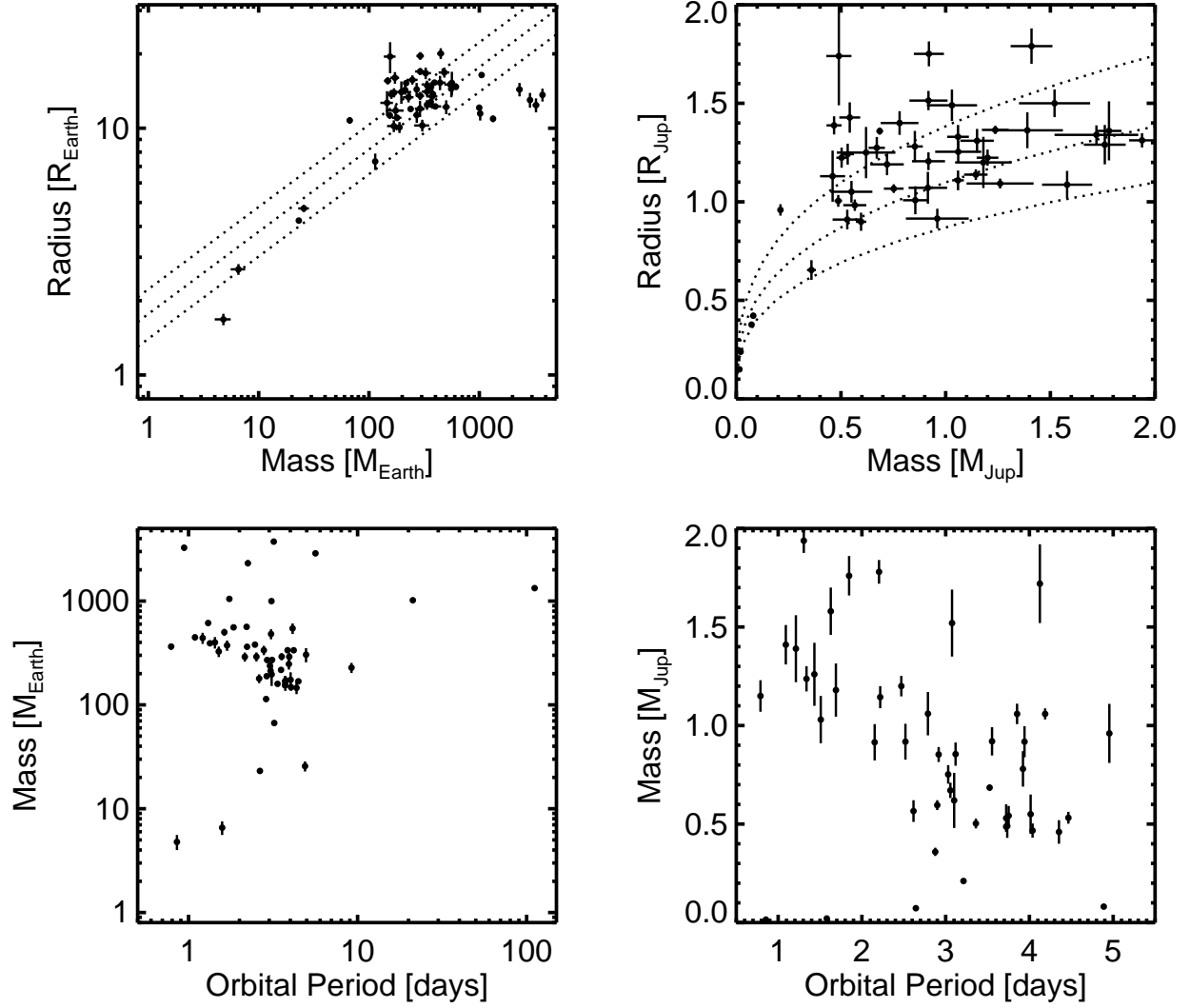
Fig. 9.— Masses, radii, and orbital periods of the transiting exoplanets. *Upper left:* Radius versus mass, on logarithmic scales. The dotted lines are loci of constant mean density (0.5, 1, and 2 g cm$^{-3}$, from top to bottom). *Upper right:* Same, but on linear scales, and with the axes restricted to highlight the gas giants that dominate the sample. *Lower left:* Mass versus orbital period, on a logarithmic scale. The two long-period outliers are HD 17156b ($P = 21$ d) and HD 80606b ($P = 111$ d). *Lower right:* Same, but on a linear scale, and with axes restricted to highlight the gas giants. The anticorrelation between mass and orbital period is evident.

radius. Most are gas giants, comparable in mass and radius to Jupiter. There are also two planets with sizes more like Neptune and Uranus, as well as two even smaller planets with sizes only a few times larger than Earth, a category that has come to be known as "super-Earths."

The two transiting super-Earths (Figure 10) were found with completely different strategies. The *CoRoT* (COnvection, ROtation, and planetary Transits) team uses a satellite equipped with a 0.27 m telescope and CCD cameras to examine fields of $\sim$10,000 stars for a few months at a time, seeking relatively short-period planets ($P \lesssim 20$ d). Along with several giant planets they have found a planet of radius 1.7 $R_\oplus$ in a 20-hour orbit around a G dwarf star, producing a transit depth of only $3.4 \times 10^{-4}$ (Léger et al. 2009). This is smaller than the detection threshold of any of the ground-based surveys, demonstrating the advantage of space-based photometry. However, it proved difficult to spectroscopically confirm that the signal is indeed due to a planet, because the host star is relatively faint and chromospherically active (Queloz et al. 2009).

Another project, called MEarth (and pronounced *mirth*), seeks transits of small planets from the ground by focusing on very small stars (M dwarfs), for which even a super-Earth would produce a transit depth of order 1%. Because such stars are intrinsically faint, one must search the whole sky to find examples bright enough for follow-up work. That is why MEarth abandoned the usual survey concept in which many stars are monitored within a single telescope's field of view. Instead they monitor M dwarf stars one at a time, using several 0.4 m telescopes. Using this strategy they found a planet of radius 2.7 $R_\oplus$ in a 1.6-day period around a star of radius 0.21 $R_\odot$ (Charbonneau et al. 2009). The large transit depth of 1.3% invites follow-up observations to study the planet's atmosphere.

At the other extreme, several transiting objects have masses greater than 10 $M_{\rm Jup}$, reviving the old debate about what should and should not be considered a planet. The radii of these massive objects are not much larger than Jupiter's radius, in agreement with predictions that between about 1–50 $M_{\rm Jup}$ the pressure due to Coulomb forces (which would give $R \propto M^{1/3}$) and electron degeneracy pressure ($R \propto M^{-1/3}$) conspire to mute the mass-dependence of the radius.

Almost all of the transiting planets have short orbital periods ($<$10 days), due to the decline in transit probability with orbital distance (equation 12). Two conspicuous exceptions are HD 17156b with $P = 21$ days (Barbieri et al. 2009), and HD 80606b with $P = 111$ days (Moutou et al. 2009, Garcia-Melendo & McCullough 2009, Fossey et al. 2009). Both of those planets were discovered by the Doppler method and found to transit through photometric follow-up observations. They were recognized as high-priority targets because both systems have highly eccentric orbits oriented in such a way as to enhance the probability of eclipses. Thus despite their long orbital periods, their periastron distances are small ($<$0.1 AU) along with all of the other known transiting planets.

## 5.2 Follow-up photometry and absolute dimensions

Follow-up observations of transits have allowed the basic transit parameters $\{\delta, T, \tau\}$ to be determined to within 1% or better, and absolute dimensions of planets to within about 5%. Compilations of system parameters are given by Torres, Winn, & Holman (2008) and Southworth (2009). The orbital periods are known with 8 significant digits in some cases. Ground-based observations have achieved a photometric precision of 250 ppm per 1 min sample, through the techniques described in Section 4.2.

A pathbreaking achievement was the *Hubble Space Telescope* light curve of HD 209458 by Brown et al. (2001), with a time sampling of 80 s and a precision of 110 ppm, without the need for comparison stars. With the *Spitzer Space Telescope* the photon noise is generally higher, but there are compensatory advantages: there is little limb-darkening at at mid-infrared wavelengths, and uninterrupted views of entire events are possible because the satellite is not in a low-earth orbit. Among the most spectacular data yet obtained in this field was the 33 hr observation by Knutson et al. (2007b) of the K star HD 189733, spanning both a transit and occultation of its giant planet. The data were gathered with *Spitzer* at a wavelength of 8 $\mu$m, and are shown in Figure 11. They not only provided extremely precise light curves of the transit and occultation, but also showed that the combined flux rises gradually in between those two events, demonstrating that the dayside is hotter than the nightside.

Among the properties of the close-in giant planets, a few patterns have emerged. The planetary mass is inversely related to the orbital period (Mazeh, Zucker, & Pont 2005). This anticorrelation has been variously attributed to selection effects, tidal interactions, and thermal evaporation of the planetary atmosphere. There is also a positive correlation between the metallicity of the host star and the inferred "core mass" of the planet (Guillot et al. 2006), by which is meant the mass of heavy elements required in models of the planetary interior that agree with the observed mass and radius. It is tempting to interpret this latter correlation as support for the core-accretion theory of planet formation.

A persistent theme in this field, and a source of controversy and speculation, is that several of the transiting giant planets have radii that are 10-50% larger than expected from models of hydrogen-helium planets, even after accounting for the intense stellar heating and selection effects (see the chapter by Correia and Laskar). Among the possible explanations for these "bloated" planets are tidal heating (see, e.g., Miller et al. 2009); unknown atmospheric constituents that efficiently trap internal heat (Burrows et al. 2007); enhanced downward convection allowing the incident stellar radiation to reach significant depth (Guillot & Showman 2002); and inhibition of convection within the planet that traps internal heat (Chabrier & Baraffe 2007).

Likewise, a few planets are observed to be *smaller* than expected for a hydrogen-helium planet with the observed mass and degree of irradiation. Some examples are
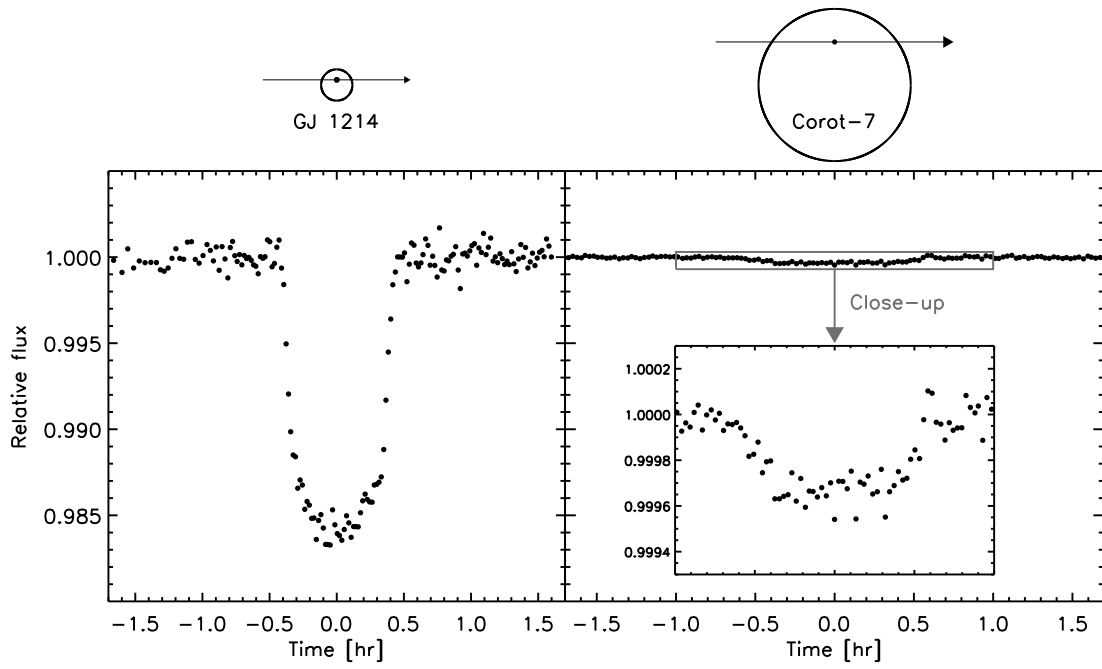
Fig. 10.— Transits of two different super-Earths, GJ 1214b (left) and CoRoT-7b (right). The planets are approximately the same size, but because GJ 1214b orbits a small star (spectral type M4.5V) its transit depth is much larger than that of CoRoT-7b, which orbits a larger star (G9V). References: Charbonneau et al. (2009), Léger et al. (2009).
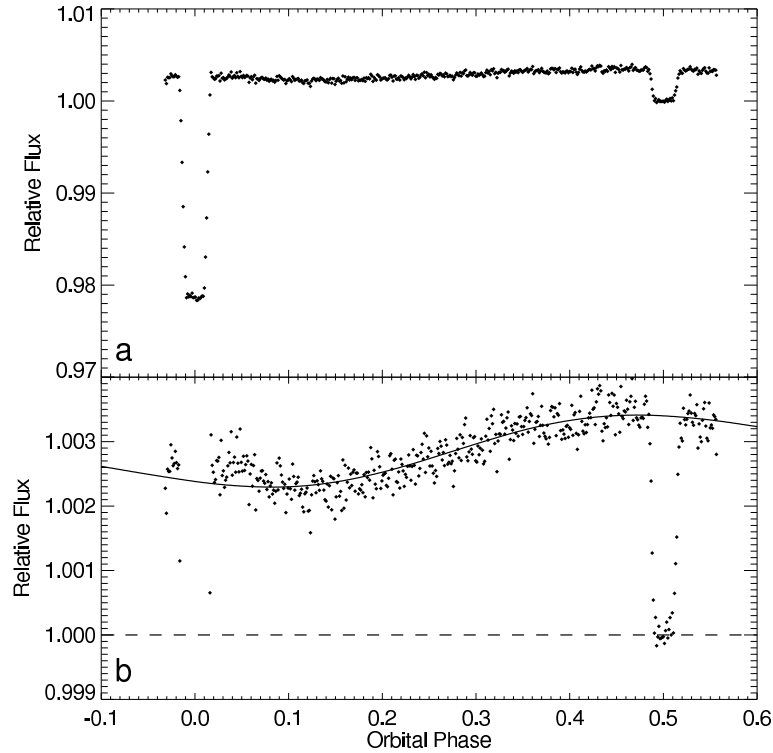


Fig. 11.— The combined 8 $\mu$m brightness of the K star HD 189733 and its giant planet, over a 33 hr interval including a transit and an occultation. The bottom panel shows the same data as the top panel but with a restricted vertical scale to highlight the gradual rise in brightness as the planet's dayside comes into view. The amplitude of this variation gives the temperature contrast between the dayside (estimated as $1211 \pm 11$ K) and the nightside ($973 \pm 33$ K). From Knutson et al. (2007b).

17

HD 149026b (Sato et al. 2005) and HAT-P-3b (Torres et al. 2007). The favored interpretation is that these planets are enriched in elements heavier than hydrogen and helium, and the increased mean molecular weight leads to a larger overall density. Some degree of enrichment might be expected because Jupiter and Saturn are themselves enriched in hevay elements relative to the Sun. However the two planets just mentioned would need to be enriched still further; in the case of HD 149026b, theoretical models suggest that the planet is 65% heavy elements by mass.

## 5.3 Atmospheric physics

Atmospheric spectra have been obtained for several gas giant planets, especially the two "hot Jupiters" with the brightest host stars, HD 209458b and HD 189733b. Both transmission and emission spectroscopy have been undertaken, mainly with the space telescopes *Hubble* and *Spitzer*. Figures 12 and 13 show examples of both transmission (transit) and emission (occultation) spectra. These observations have stimulated much theoretical work on exoplanetary atmospheres (see the chapters by Chambers and by D'Angelo et al. for more details than are presented here).

This enterprise began with the optical detection of neutral sodium in a transmission spectrum of HD 209458b by Charbonneau et al. (2002). For that same planet, Vidal-Madjar et al. (2003) measured an enormous transit depth of $(15 \pm 4)$% within an ultraviolet bandpass bracketing the wavelength of the Lyman-$\alpha$ transition, which they attributed to neutral hydrogen gas being blown off the planet. For HD 189733b, a rise in transit depth toward shorter wavelengths was observed by Pont et al. (2007) and interpreted as Rayleigh scattering in the planet's upper atmosphere.

Recent attention has turned to infrared wavelengths, where molecules make their imprint. In the emission spectra, departures from a blackbody spectrum have been interpreted as arising from water, methane, carbon monoxide, and carbon dioxide (see, e.g., Grillmair et al. 2008, Swain et al. 2009). Absorption features in transmission spectra have been interpreted as arising from water and methane (see, e.g., Swain et al. 2008, Tinetti et al. 2007).

Despite these impressive achievements, many issues regarding the atmospheres of hot Jupiters remain unsettled. Controversies arise because spectral features are observed with a low signal-to-noise ratio and are not always reproducible, as illustrated in Figure 12. This is understandable, as the observers have pushed the instruments beyond their design specifications to make these demanding measurements. In addition, the theoretical interpretation of the spectra is in a primitive state. A published spectrum is usually accompanied by a model that fits the data, but left unanswered are whether the model is unique and how well-constrained are its parameters. Recent work by Madhusudhan & Seager (2009) addresses this problem.

One theme that has arisen in the last few years is that some hot Jupiters have an *inversion layer* in their upper at-

mospheres, within which the temperature rises with height instead of the usual decline. The evidence for an inversion layer is emission in excess of a blackbody spectrum between 4–8 $\mu$m, where excess *absorption* was expected due to water vapor. The interpretation is that water is seen in emission because it exists in a hot, tenuous stratosphere.

Hot stratospheres develop when starlight is strongly absorbed by some species at low pressure (at high altitude) where the atmosphere does not radiate efficiently. The identity of this absorber in hot Jupiter atmospheres has been a topic of debate. Gaseous titanium oxide and vanadium oxide are candidates (Hubeny et al. 2003), as are photochemically-produced sulfur compounds (Zahnle et al. 2009). Meanwhile observers are searching for correlations between the presence or absence of an inversion layer, the degree of stellar irradiation, the magnitude of the day-night temperature difference, and other observable properties.

A few of the known planets have highly eccentric orbits and small periastron distances, and are therefore subject to highly variable stellar irradiation. Observers have monitored the planetary thermal emission following periastron passages, to gauge the amplitude and timescale of the thermal response to stellar heating. In the most extreme case, Laughlin et al. (2009) watched the effective temperature of the giant planet HD 80606b rise from about 800 K to 1500 K after periastron passage, and inferred that the characteristic radiative timescale of the upper atmosphere is about 4.5 hr.

Although the thermal emission from hot Jupiters has been detected in many cases, at infrared and optical wavelengths, there has been no unambiguous detection of starlight *reflected* from the planetary atmosphere. The best resulting upper limit on the visual planetary albedo is 0.17 (with $3\sigma$ confidence), for the case of HD 209458b (Rowe et al. 2008). This rules out highly reflective clouds of the sort that give Jupiter its visual albedo of 0.5. However, the limits have not been of great interest to the theorists, who predicted all along that the visual albedos of hot Jupiters would be very small.

## 5.4 Tidal evolution and migration

Almost all of the known transiting planets are close enough to their parent stars for tidal effects to be important. The tidal bulges on the star and planet provide "handles" for the bodies to torque each other, and tidal friction slowly drains energy from the system (see the chapter by Fabrycky). For a typical hot Jupiter, the sequence of events is expected to be as follows: (i) Over $\sim 10^6$ yr, the planet's rotational period is synchronized with its orbital period, and its obliquity (the angle between its rotational and orbital angular momentum vectors) is driven to zero. (ii) Over $\sim 10^9$ yr, the orbit is circularized. (iii) After $\sim 10^{12}$ yr (i.e. not yet), the stellar rotational period is synchronized with the orbital period, the stellar obliquity is driven to zero, and the orbit decays, leading to the engulfment of the planet.
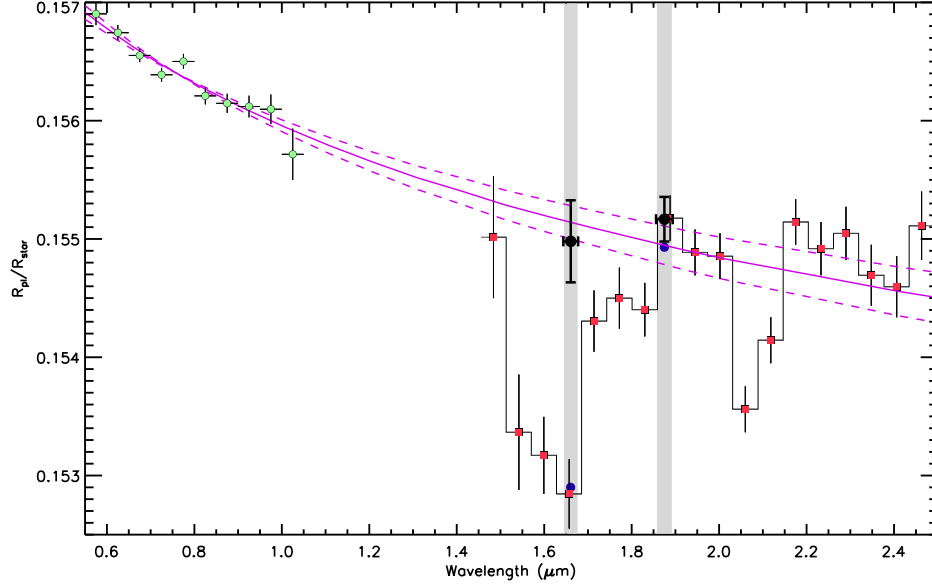
Fig. 12.— Transmission (transit) spectroscopy of the gas giant HD 189733b, using the *Hubble Space Telescope*. The symbols with errors bars are measurements of the effective planet-to-star radius ratio as a function of wavelength. The dip at 1.6 $\mu$m was interpreted as evidence for water, and the rise at 2.1 $\mu$m as evidence for methane (Swain et al. 2008). However, subsequent observations at 1.7 $\mu$m and 1.9 $\mu$m, shown with darker symbols and gray bands, disagree with the earlier results and are consistent with a Rayleigh scattering model (solid and dashed curves). From Sing et al. (2009).
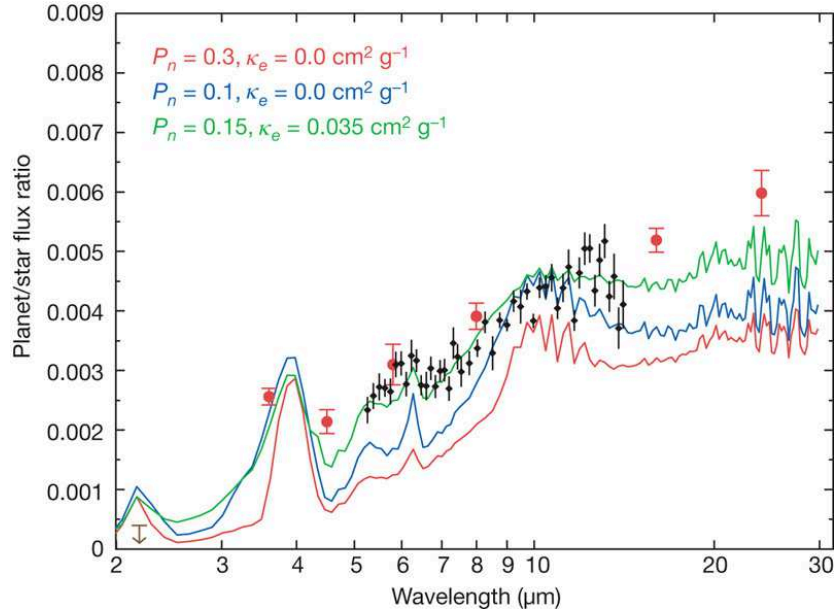


Fig. 13.— Occultation spectroscopy of the gas giant HD 189733b, using the *Spitzer Space Telescope*. The points show measurements of the flux density ratio of the planet and star as a function of wavelength. The smaller and finer-sampled points are based on observations with a dispersive spectrograph while the larger points are based on broadband filter photometry. The three lines show the outputs of model atmospheres with varying choices for the parameters $P_n$, specifying the efficiency of heat transfer from dayside to nightside, and $\kappa_e$, specifying the opacity of a putative high-altitude absorbing species. From Grillmair et al. (2008).

The timescales for these processes are highly uncertain, and more complex histories are possible if there are additional planets in the system or if the planet's internal structure is strongly affected by tidal heating.

Tidal circularization is implicated by the fact that planets with orbital periods shorter than ~10 days tend to have smaller orbital eccentricities than longer-period planets. This fact was already known from Doppler surveys, but for eclipsing planets the eccentricities can be measured more precisely (see Section 3.2). It is possible that the "bloating" of some of the close-in giant planets (Section 5.3) is related to the heat that was produced during the circularization process, or that may still be ongoing.

As for tidal synchronization, observations with *Spitzer* have revealed planets with a cold side facing away from the star and a hot side facing the star (see Figure 11). This could be interpreted as evidence for synchronization, although it is not definitive, because it is also possible that the heat from the star is re-radiated too quickly for advection to homogenize the upper atmosphere of the planet.

Tidal decay of the orbit would be observable as a gradual decline in the orbital period (Sasselov 2003). For most systems the theoretical timescale for tidal decay is much longer than the age of the star, and indeed no evidence for this process has been found. However in at least one case (WASP-18b; Hellier et al. 2009) the theoretical timescale for tidal decay is much *shorter* than the stellar age, because of the large planetary mass and short orbital period. The existence of this system suggests that the theoretical expectations were wrong and dissipation is slower in reality.

Likewise, in most cases one would not expect that enough time has elapsed for tides to modify the star's spin rate or orientation (Barker & Ogilvie 2009). This suggests that the measurements of the projected spin-orbit angle using the RM effect (Section 3.5) should be interpreted in the context of planet formation and evolution rather than tides. A close spin-orbit alignment is expected because a star and its planets inherit their angular momentum from a common source: the protostellar disk. However, for hot Jupiters there is the complication that they presumably formed at larger distances and "migrated" inward through processes that are poorly understood. Some of the migration theories predict that the original spin-orbit alignment should be preserved, while others predict occasionally large misalignments. For example, tidal interactions with the protoplanetary disk (see chapter by Showman et al.) should drive the system into close alignment (Marzari & Nelson 2009), while planet-planet scattering or Kozai oscillations with tidal friction (see chapter by Fabrycky) should result in misaligned systems.

The projected spin-orbit angle has been measured for about 20 exoplanets, all of them close-in giants. Some examples of data are shown in Figure 14. In many cases the results are consistent with good alignment, with measurement precisions ranging from 1–20° (for a recent summary, see Fabrycky & Winn 2009). However there are now at least 4 clear cases of misaligned systems. One such case is

XO-3b, a massive planet in a close-in eccentric orbit that is tilted by more than 30° with respect to the stellar equator (Hébrard et al. 2008, Winn et al. 2009a). Even more dramatic is HAT-P-7b, for which the planetary orbit and stellar spin axis are tilted by more than 86° (Winn et al. 2009b, Narita et al. 2009). The planetary orbit is either polar (going over the north and south poles of the star) or retrograde (revolving in the opposite direction as the star is rotating). Another possible retrograde system is WASP-17b (Anderson et al. 2009).

## 6. FUTURE PROSPECTS

Eclipses are the "here and now" of exoplanetary science. It seems that every month, someone reports a startling observational feat, describes a creative new application of eclipse data, or proposes an ambitious survey to find ever-larger numbers of ever-smaller transiting planets. Keeping up with the field leaves one breathless, and wary of making predictions.

The only safe bet is that the *Kepler* space mission will have a major impact. In March 2009, the *Kepler* satellite was launched into an an Earth-trailing orbit where it will stare at a single field of $10^5$ stars for at least 3.5 yr, seeking Earth-like planets in Earth-like orbits around Sun-like stars (Borucki et al. 2003). *Kepler* will end our obsession with close-in, tidally-influenced, strongly-irradiated giant planets. At last it will be possible to study eclipses of multitudes of longer-period and smaller-radius planets. Stellar heating will not confound models of their atmospheres or interiors, and tidal effects will not confound the interpretation of their orbital properties.

Many of *Kepler*'s discoveries will be small enough to have solid surfaces, making it possible to measure masses and radii of rocky exoplanets. The mission's highest priority goal is to determine the abundance of terrestrial planets in the "habitable zones" of their parent stars, defined as the range of orbital distances within which water could exist in liquid form on the surface of a rocky planet. The abundance of such planets is a key input to the "Drake equation" as well as to theories of planet formation and to the designs of future missions that will find and study the nearest examples.

The precision of space-based photometry will also be put to good use to detect a host of subtle effects that have been described in the literature but not yet observed. Already, data from the *Kepler* and *CoRoT* satellites have been used to detect occultations in visible light, as opposed to infrared (Borucki et al. 2009, Snellen et al. 2009), although in both cases the signal is attributed mainly to thermal emission rather than the elusive reflected component.

Many investigators will seek to detect short-term variations in the times, durations, and depths of transits due to gravitational perturbations by additional planets, as mentioned in Section 3.2 and discussed further in the chapter by Fabrycky. In particular, *Kepler* might find habitable planets not only by detecting their transits, but also by observing
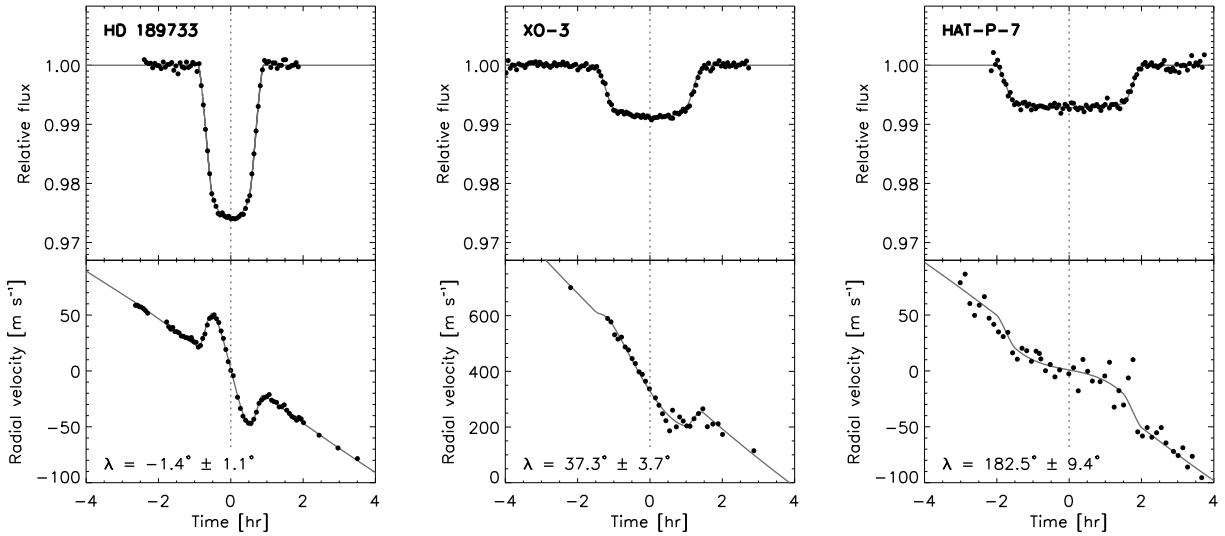
Fig. 14.— Examples of data used to measure the projected spin-orbit angle $\lambda$. The top panels show transit photometry, and the bottom panels show the apparent radial velocity of the star, including both orbital motion and the anomalous Doppler shift (the Rossiter-McLaughlin effect). The left panels show a well-aligned system and the middle panels show a misaligned system. The right panels show a system for which the stellar and orbital "north poles" are nearly *antiparallel* on the sky, indicating that the planet's orbit is either retrograde or polar (depending on the unknown inclination of the stellar rotation axis). References: Winn et al. (2006; 2009a,b).

their effects on other transiting planets. The same principle can be used to detect habitable "exomoons" (Kipping et al. 2009) or habitable planets at the Trojan points (Lagrange L4 and L5) in the orbits of more massive planets (Ford & Gaudi 2006, Madhusudhan & Winn 2009).

Longer-term orbital perturbations should also be measurable, due to additional bodies (Miralda-Escudé 2002) or relativistic precession (Jordán & Bakos 2008, Pál & Kocsis 2008). For very close-in planets, the orbital precession rate should be dominated by the effects of the planetary tidal bulge, which in turn depends on the deformability of the planet. This raises the prospect of using the measured precession rate to infer some aspects of the planet's interior structure (Ragozzine & Wolf 2009).

In addition, the precise form of the transit light curve depends on the shape of the planet's silhouette. With precise enough photometry it may be possible to detect the departures from sphericity due to rings (Barnes & Fortney 2004) or rotation (Seager & Hui 2002, Barnes & Fortney 2003). Already it has been shown that HD 189733b is less oblate than Saturn (Carter & Winn 2009b), as expected if the planet's rotation period is synchronized with its 2.2-day orbit (slower than Saturn's 11 hr rotation period). Soon we will have a sample of transiting planets with larger orbital distances, for which synchronization is not expected and which may therefore be rotating quickly enough for the oblateness to be detectable.

Another prize that remains to be won is the discovery of a system with more than one transiting planet. This would give empirical constraints on the mutual inclination of exoplanetary orbits (Nesvorný 2009), as well as esti-

mates of the planetary masses that are independent of the stellar mass, through the observable effects of planet-planet gravitational interactions. Already there are a few cases in which there is evidence for a second planet around a star that is known to have a transiting planet (see, e.g., Bakos et al. 2009), but in none of those cases is it known whether the second planet also transits.

Ground-based transit surveys will still play an important role by targeting brighter stars over wider fields than *CoRoT* and *Kepler*. With brighter stars it is easier to rule out false positives, and to measure the planetary mass through radial-velocity variations of the host star. For the smallest planets around the relatively faint stars in the *CoRoT* and *Kepler* fields this will be difficult. Bright stars also offer more photons for the high-precision follow-up investigations that make eclipses so valuable.

Ground-based surveys will continue providing such targets, and in particular will mine the southern sky, which is comparatively unexplored. Two contenders are the Super-WASP and HAT-South surveys, which will aim to improve their photometric precision and discover many Neptune-sized or even smaller planets in addition to the gas giants. The MEarth project, mentioned in Section 5.1, is specifically targeting small and low-luminosity stars because of the less stringent requirements on photometric precision and because the habitable zones occur at smaller orbital distances, making transits more likely and more frequent (Nutzman & Charbonneau 2008).

An attractive idea is to design a survey with the fine photometric precision that is possible from space, but that would somehow survey the brightest stars on the sky in-

stead of those within a narrow field of view. Several mission concepts are being studied: the *Transiting Exoplanet Survey Satellite* (Deming et al. 2009) and the *PLATO* mission (Lindberg et al. 2009) would tile the sky with the fields-of-view of small cameras, while *LEAVITT* would have a series of telescopes on a spinning platform (Olling 2007). Another concept is to deploy an armada of "nanosatellites" to target individual stars (S. Seager, priv. comm. 2009).

Each time a terrestrial planet is found transiting a bright star, a period of intense anticipation will ensue, as astronomers try to characterize its atmosphere through transmission or emission spectroscopy. The anticipation will be especially keen for any planets in the habitable zone of their parent stars, which may reveal water or other molecules considered important for life. Attaining the necessary signal-to-noise ratio will be excruciating work, and may require the *James Webb Space Telescope* or an even more capable special-purpose instrument.

Transits and occultations have had a disproportionate impact early in the history of exoplanetary science. This is mainly because of the unexpected existence of close-in giant planets, and their high transit probabilities. In the coming years, other techniques such as astrometry, microlensing, and spatially-resolved imaging will mature and give a more complete accounting of exoplanetary systems. Still, in closing, let us recall that most of our most fundamental and precise information about *stars* comes from eclipsing systems, even after more than a century of technological development since eclipses were first observed. The same is likely to be true for exoplanets.

## REFERENCES

Agol, E., Steffen, J., Sari, R., Clarkson, W. (2005) On detecting terrestrial planets with timing of giant planet transits. *Mon. Not. Roy. Astr. Soc. 359*, 567-579.

Alonso, R., and 11 colleagues (2004) TrES-1: The Transiting Planet of a Bright K0 V Star. *Astrophys. J. 613*, L153-L156.

Anderson, D. R., and 20 colleagues (2010) WASP-17b: An Ultra-Low Density Planet in a Probable Retrograde Orbit. *Astrophysical Journal 709*, 159-167.

Baines, E. K., van Belle, G. T., ten Brummelaar, T. A., McAlister, H. A., Swain, M., Turner, N. H., Sturmann, L., Sturmann, J. (2007) Direct Measurement of the Radius and Density of the Transiting Exoplanet HD 189733b with the CHARA Array. *Astroph. J. 661*, L195-L198.

Bakos, G. Á., and 18 colleagues (2009) HAT-P-13b,c: A Transiting Hot Jupiter with a Massive Outer Companion on an Eccentric Orbit. *Astrophysical Journal 707*, 446-456.

Bakos, G. Á., and 18 colleagues (2007) HAT-P-1b: A Large-Radius, Low-Density Exoplanet Transiting One Member of a Stellar Binary. *Astrophys. J. 656*, 552-559.

Barbieri, M., and 10 colleagues (2007) HD 17156b: a transiting planet with a 21.2-day period and an eccentric orbit. *Astronomy and Astrophysics 476*, L13-L16.

Barker, A. J., Ogilvie, G. I. (2009) On the tidal evolution of Hot Jupiters on inclined orbits. *Mon. Not. Roy. Astr. Soc. 395*, 2268-2287.

Barnes, J. W., Fortney, J. J. (2003) Measuring the Oblateness and Rotation of Transiting Extrasolar Giant Planets. *Astrophysical Journal 588*, 545-556.

Barnes, J. W., Fortney, J. J. (2004) Transit Detectability of Ring Systems around Extrasolar Giant Planets. *Astrophysical Journal 616*, 1193-1203.

Beatty, T. G., & Gaudi, B. S. (2008) Predicting the Yields of Photometric Surveys for Transiting Extrasolar Planets, *Astroph. J., 686*, 1302-1330.

Borucki, W. J., and 24 colleagues (2009) Kepler's Optical Phase Curve of the Exoplanet HAT-P-7b. *Science 325*, 709.

Brown, T. M. (2001) Transmission Spectra as Diagnostics of Extrasolar Giant Planet Atmospheres. *Astroph. J. 553*, 1006-1026.

Brown, T. M., Charbonneau, D., Gilliland, R. L., Noyes, R. W., Burrows, A. (2001) Hubble Space Telescope Time-Series Photometry of the Transiting Planet of HD 209458. *Astrophysical Journal 552*, 699-709.

Borucki, W. J., and 12 colleagues (2003) The Kepler mission: a wide-field-of-view photometer designed to determine the frequency of Earth-size planets around solar-like stars. *Soc. Photo-Optical Instr. Eng. (SPIE) Conf. Ser. 4854*, 129-140.

Burke, C. J., and 17 colleagues (2007) XO-2b: Transiting Hot Jupiter in a Metal-rich Common Proper Motion Binary. *Astrophysical Journal 671*, 2115-2128.

Burrows, A., Hubeny, I., Budaj, J., Hubbard, W. B. (2007) Possible Solutions to the Radius Anomalies of Transiting Giant Planets. *Astrophys. J. 661*, 502-514.

Carciofi, A. C. & Magalhães, A. M. (2005) The Polarization Signature of Extrasolar Planet Transiting Cool Dwarfs. *Astrophs. J. 635*, 570-577.

Carter, J. A., Yee, J. C., Eastman, J., Gaudi, B. S., Winn, J. N. (2008) Analytic Approximations for Transit Light-Curve Observables, Uncertainties, and Covariances. *Astrophysical Journal 689*, 499-512.

Carter, J. A., Winn, J. N., Gilliland, R., Holman, M. J. (2009) Near-Infrared Transit Photometry of the Exoplanet HD 149026b. *Astrophysical Journal 696*, 241-253.

Carter, J. A., Winn, J. N. (2009a) Parameter Estimation from Time-series Data with Correlated Errors: A Wavelet-based Method and its Application to Transit Light Curves. *Astrophysical Journal 704*, 51-67.

Carter, J. A., Winn, J. N. (2009b) Empirical Constraints on the Oblateness of an Exoplanet. *Astrophysical Journal, 709*, 1219.

Chabrier, G., Baraffe, I. 2007. Heat Transport in Giant (Exo)planets: A New Perspective. *Astrophysical Journal 661*, L81-L84.

Charbonneau, D., Brown, T. M., Latham, D. W., Mayor, M. (2000) Detection of Planetary Transits Across a Sun-like Star. *Astrophys. J. 529*, L45-L48.

Charbonneau, D., Brown, T. M., Noyes, R. W., Gilliland, R. L. (2002) Detection of an Extrasolar Planet Atmosphere. *Astrophys. J. 568*, 377-384.

Charbonneau, D. and 18 colleagues (2009) A super-Earth transiting a nearby low-mass star. *Nature 462*, 891-894.

Claret, A. (2004) A new non-linear limb-darkening law for LTE stellar atmosphere models. III. Sloan filters: Calculations for $-5.0 \leq \log [M/H] \leq +1$, 2000 K $\leq T_{\mathrm{eff}} \leq$ 50000 K at

several surface gravities. *Astron. Astroph. 428*, 1001-1005.

Claret, A. (2009) Does the HD 209458 planetary system pose a challenge to the stellar atmosphere models? *Astronomy and Astrophysics 506*, 1335-1340.

Collier Cameron, A., and 31 colleagues (2007) Efficient identification of exoplanetary transit candidates from SuperWASP light curves. *Monthly Notices of the Royal Astronomical Society 380*, 1230-1244.

de Kort, J. J. M. A. (1954) Upper and lower limits for the eccentricity and longitude of periastron of an eclipsing binary. *Ricerche Astronomiche 3*, 109-118.

Deming, D., and 11 colleagues (2009) Discovery and Characterization of Transiting Super Earths Using an All-Sky Transit Survey and Follow-up by the James Webb Space Telescope. *Publications of the Astronomical Society of the Pacific 121*, 952-967.

Everett, M. E. & Howell, S. B. (2001) A Technique for Ultrahigh-Precision CCD Photometry. *Publ. Astron. Soc. Pacific 113*, 1428-1435.

Fabrycky, D. C., Winn, J. N. (2009) Exoplanetary Spin-Orbit Alignment: Results from the Ensemble of Rossiter-McLaughlin Observations. *Astroph. J. 696*, 1230-1240.

Ford, E. B., Gaudi, B. S. (2006) Observational Constraints on Trojans of Transiting Extrasolar Planets. *Astrophysical Journal 652*, L137-L140.

Fossey, S. J., Waldmann, I. P., Kipping, D. M. (2009) Detection of a transit by the planetary companion of HD 80606. *Monthly Notices of the Royal Astronomical Society 396*, L16-L20.

Garcia-Melendo, E., McCullough, P. R. (2009) Photometric Detection of a Transit of HD 80606b. *Astrophysical Journal 698*, 558-561.

Gaudi, B. S. (2005) On the Size Distribution of Close-in Extrasolar Giant Planets. *Astroph. J. 628*, L73-L76

Gaudi, B. S., Seager, S., & Mallen-Ornelas, G. (2005) On the Period Distribution of Close-in Extrasolar Giant Planets. *Astroph. J. 623*, 472-481.

Gaudi, B. S., Winn, J. N. (2007) Prospects for the Characterization and Confirmation of Transiting Exoplanets via the Rossiter-McLaughlin Effect. *Astroph. J. 655*, 550-563.

Gilliland, R. L., & Brown, T. M. (1988) Time-resolved CCD photometry of an ensemble of stars. *Publ. Astron. Soc. Pacific 100*, 754-765.

Gilliland, R. L., and 23 colleagues (2000) A Lack of Planets in 47 Tucanae from a Hubble Space Telescope Search. *Astrophys. J. 545*, L47-L51.

Gillon, M., Demory, B.-O., Barman, T., Bonfils, X., Mazeh, T., Pont, F., Udry, S., Mayor, M., Queloz, D. (2007) Accurate Spitzer infrared radius measurement for the hot Neptune GJ 436b. *Astronomy and Astrophysics 471*, L51-L54.

Giménez, A. (2007) Equations for the analysis of the light curves of extra-solar planetary transits. *Astron. Astrophys. 474*, 1049-1049.

Gregory, P. C. (2005) *Bayesian Logical Data Analysis for the Physical Sciences: A Comparative Approach with Mathematica Support*, Cambridge University Press

Grillmair, C. J., Burrows, A., Charbonneau, D., Armus, L., Stauffer, J., Meadows, V., van Cleve, J., von Braun, K., Levine, D. (2008) Strong water absorption in the dayside emission spectrum of the planet HD189733b. *Nature 456*, 767-769.

Guillot, T., Santos, N. C., Pont, F., Iro, N., Melo, C., Ribas, I. (2006) A correlation between the heavy element content of transiting extrasolar planets and the metallicity of their parent

stars. *Astron. Astroph. 453*, L21-L24.

Guillot, T., Showman, A. P. (2002) Evolution of "51 Pegasus b-like" planets. *Astronomy and Astrophysics 385*, 156-165.

Hébrard, G., and 22 colleagues (2008) Misaligned spin-orbit in the XO-3 planetary system? *Astron. Astrophys. 488*, 763-770.

Hellier, C., and 22 colleagues (2009) An orbital period of 0.94 days for the hot-Jupiter planet WASP-18b. *Nature 460*, 1098-1100.

Henry, G. W., Marcy, G. W., Butler, R. P., Vogt, S. S. (2000) A Transiting "51 Peg-like" Planet. *Astrophys. J. 529*, L41-L44

Hilditch, R. W. (2001) *An Introduction to Close Binary Stars* (Cambridge, UK: Cambridge University Press)

Holman, M. J., Murray, N. W. (2005) The Use of Transit Timing to Detect Terrestrial-Mass Extrasolar Planets. *Science 307*, 1288-1291.

Holman, M. J., Winn, J. N., Latham, D. W., O'Donovan, F. T., Charbonneau, D., Bakos, G. A., Esquerdo, G. A., Hergenrother, C., Everett, M. E., Pál, A. (2006) The Transit Light Curve Project. I. Four Consecutive Transits of the Exoplanet XO-1b. *Astrophysical Journal 652*, 1715-1723.

Horne, K. (2003) Status aand Prospects of Planetary Transit Searches: Hot Jupiters Galore. in *Scientific Frontiers in Research on Extrasolar Planets*, ed. D. Deming and S. Seager, ASP Conference Series Vol. 294 (San Francisco: ASP), p. 361-370.

Howell, S. B. (2006) *Handbook of CCD astronomy* (Cambridge, UK: Cambridge Univ. Press), 2nd ed.

Hubeny, I., Burrows, A., Sudarsky, D. (2003) A Possible Bifurcation in Atmospheres of Strongly Irradiated Stars and Planets. *Astrophysical Journal 594*, 1011-1018.

Jordán, A., Bakos, G. Á. (2008) Observability of the General Relativistic Precession of Periastra in Exoplanets. *Astrophys. J. 685*, 543-552.

Kallrath, J. & Milone, E. F. (2009) *Eclipsing Binary Stars: Modeling and Analysis* (New York: Springer-New York), 2nd ed., in press

Kane, S. R. (2007) Detectability of exoplanetary transits from radial velocity surveys. *Mon. Not. Roy. Astr. Soc. 380*, 1488-1496.

Kipping, D. M. (2008) Transiting planets – light-curve analysis for eccentric orbits. *Mon. Not. Roy. Astr. Soc. 389*, 1383-1390.

Kipping, D. M. (2009) Transit timing effects due to an exomoon. *Mon. Not. Roy. Astr. Soc. 392*, 181-189.

Kjeldsen, H. & Frandsen, S. (1992) High-precision time-resolved CCD photometry. *Publ. Astron. Soc. Pacific 104*, 413-434.

Knutson, H. A., Charbonneau, D., Noyes, R. W., Brown, T. M., Gilliland, R. L. (2007a) Using Stellar Limb-Darkening to Refine the Properties of HD 209458b. *Astrophys. J. 655*, 564-575.

Knutson, H. A., Charbonneau, D., Allen, L. E., Fortney, J. J., Agol, E., Cowan, N. B., Showman, A. P., Cooper, C. S., Megeath, S. T. (2007b) A map of the day-night contrast of the extrasolar planet HD 189733b. *Nature 447*, 183-186.

Kopal, Z. (1979) Language of the stars: A discourse on the theory of the light changes of eclipsing variables. *Astrophysics and Space Science Library 77*, Kluwer, Dordrecht.

Kovács, G., Zucker, S., Mazeh, T. (2002) A box-fitting algorithm in the search for periodic transits. *Astronomy and Astrophysics 391*, 369-377.

Kovács, G., Bakos, G., Noyes, R. W. 2005. A trend filtering algorithm for wide-field variability surveys. *Monthly Notices of the Royal Astronomical Society 356*, 557-567.

Laughlin, G., Deming, D., Langton, J., Kasen, D., Vogt, S., But-

ler, P., Rivera, E., Meschiari, S. (2009) Rapid heating of the atmosphere of an extrasolar planet. *Nature 457*, 562-564.

Léger, A., and 160 colleagues (2009) Transiting exoplanets from the CoRoT space mission. VIII. CoRoT-7b: the first super-Earth with measured radius. *Astronomy and Astrophysics 506*, 287-302.

Lindberg, R., Stankov, A., Fridlund, M., Rando, N. (2009) Current status of the assessment of the ESA Cosmic Vision mission candidate PLATO. *Proceedings of the SPIE 7440*, 7440Z-1 to 7440Z-12

Madhusudhan, N., Seager, S. (2009) A Temperature and Abundance Retrieval Method for Exoplanet Atmospheres. *Astrophysical Journal 707*, 24-39.

Madhusudhan, N., Winn, J. N. (2009) Empirical Constraints on Trojan Companions and Orbital Eccentricities in 25 Transiting Exoplanetary Systems. *Astrophysical Journal 693*, 784-793.

Mandel, K., Agol, E. (2002) Analytic Light Curves for Planetary Transit Searches. *Astrophys. J. 580*, L171-L175.

Marzari, F., Nelson, A. F. (2009) Interaction of a Giant Planet in an Inclined Orbit with a Circumstellar Disk. *Astrophysical Journal 705*, 1575-1583.

Mazeh, T., and 19 colleagues (2000) The Spectroscopic Orbit of the Planetary Companion Transiting HD 209458. *Astrophysical Journal 532*, L55-L58.

Mazeh, T., Zucker, S., Pont, F. (2005) An intriguing correlation between the masses and periods of the transiting planets. *Mon. Not. Roy. Astr. Soc. 356*, 955-957.

McCullough, P. R., Stys, J. E., Valenti, J. A., Fleming, S. W., Janes, K. A., Heasley, J. N. (2005) The XO Project: Searching for Transiting Extrasolar Planet Candidates. *Publ. Astron. Soc. Pacific 117*, 783-795.

Miller, N., Fortney, J. J., Jackson, B. (2009) Inflating and Deflating Hot Jupiters: Coupled Tidal and Thermal Evolution of Known Transiting Planets. *Astrophysical Journal 702*, 1413-1427.

Miralda-Escudé, J. (2002) Orbital Perturbations of Transiting Planets: A Possible Method to Measure Stellar Quadrupoles and to Detect Earth-Mass Planets. *Astrophys. J. 564*, 1019-1023.

Moutou, C., and 21 colleagues (2009) Photometric and spectroscopic detection of the primary transit of the 111-day-period planet HD 80606b. *Astronomy and Astrophysics 498*, L5-L8.

Narita, N., Sato, B., Hirano, T., Tamura, M. (2009) First Evidence of a Retrograde Orbit of a Transiting Exoplanet HAT-P-7b. *Publications of the Astronomical Society of Japan 61*, L35-L40.

Nesvorný, D. (2009) Transit Timing Variations for Eccentric and Inclined Exoplanets. Astrophysical Journal 701, 1116-1122.

Nutzman, P., Charbonneau, D. (2008) Design Considerations for a Ground-Based Transit Search for Habitable Planets Orbiting M Dwarfs. *Publications of the Astronomical Society of the Pacific 120*, 317-327.

O'Donovan, F. T., Charbonneau, D., Alonso, R., Brown, T. M., Mandushev, G., Dunham, E. W., Latham, D. W., Stefanik, R. P., Torres, G., Everett, M. E. (2007) Outcome of Six Candidate Transiting Planets from a TrES Field in Andromeda. *Astrophys. J. 662*, 658-668.

Olling, R. P. (2007) LEAVITT: A MIDEX-class Mission for Finding and Characterizing 10,000 Transiting Planets in the Solar Neighborhood. ArXiv e-prints arXiv:0704.3072.

Pál, A., Kocsis, B. (2008) Periastron precession measurements in transiting extrasolar planetary systems at the level of general relativity. *Monthly Notices of the Royal Astronomical Society 389*, 191-198.

Pepper, J., Gould, A., Depoy, D. L. (2003) Using All-Sky Surveys to Find Planetary Transits. *Acta Astronomica 53*, 213-228.

Pollacco, D. L., and 27 colleagues (2006) The WASP Project and the SuperWASP Cameras. *Publ. Astron. Soc. Pacific 118*, 1407-1418.

Pont, F., Zucker, S., Queloz, D. (2006) The effect of red noise on planetary transit detection. *Monthly Notices of the Royal Astronomical Society 373*, 231-242.

Pont, F., Knutson, H., Gilliland, R. L., Moutou, C., Charbonneau, D. (2008) Detection of atmospheric haze on an extrasolar planet: the 0.55-1.05 $\mu$m transmission spectrum of HD 189733b with the Hubble Space Telescope. *Mon. Not. Roy. Astr. Soc. 385*, 109-118.

Press, W. H., Teukolsky, S. A., Vetterling, W. T., & Flannery, B. P. (2007) *Numerical Recipes: The Art of Scientific Computing*, 3rd ed., Cambridge University Press

Queloz, D., and 39 colleagues (2009) The CoRoT-7 planetary system: two orbiting super-Earths. *Astronomy and Astrophysics 506*, 303-319.

Rabus, M., Alonso, R., Belmonte, J. A., Deeg, H. J., Gilliland, R. L., Almenara, J. M., Brown, T. M., Charbonneau, D., Mandushev, G. (2009) A cool starspot or a second transiting planet in the TrES-1 system? *Astronomy and Astrophysics 494*, 391-397.

Ragozzine, D., Wolf, A. S. (2009) Probing the Interiors of very Hot Jupiters Using Transit Light Curves. *Astrophysical Journal 698*, 1778-1794.

Reiger, S. H. (1963) Starlight scintillation and atmospheric turbulence. *Astronomical Journal 68*, 395.

Rowe, J. F., and 10 colleagues (2008) The Very Low Albedo of an Extrasolar Planet: MOST Space-based Photometry of HD 209458. *Astrophysical Journal 689*, 1345-1353.

Russell, H. N. (1948) The royal road of eclipses. *Harvard Coll. Obs. Monograph 7*, 181-209.

Ryan, P., Sandler, D. (1998) Scintillation Reduction Method for Photometric Measurements. *Publications of the Astronomical Society of the Pacific 110*, 1235-1248.

Sackett, P. (1999) Searching for Unseen Planets via Occultation and Microlensing, in *Planets Outside the Solar System: Theory and Observations* (J.-M. Mariotti and D. Alloin, eds.), p. 189, Kluwer, Dordrecht.

Sasselov, D. D. (2003) The New Transiting Planet OGLE-TR-56b: Orbit and Atmosphere. *Astrophysical Journal 596*, 1327-1331.

Sato, B., and 20 colleagues (2005) The N2K Consortium. II. A Transiting Hot Saturn around HD 149026 with a Large Dense Core. *Astrophys. J. 633*, 465-473.

Seager, S., Hui, L. (2002) Constraining the Rotation Rate of Transiting Extrasolar Planets by Oblateness Measurements. *Astroph. J. 574*, 1004-1010.

Seager, S., Mallén-Ornelas, G. (2003) A Unique Solution of Planet and Star Parameters from an Extrasolar Planet Transit Light Curve. *Astroph. J. 585*, 1038-1055.

Seager, S., Sasselov, D. D. (2000) Theoretical Transmission Spectra during Extrasolar Giant Planet Transits. *Astroph. J. 537*, 916-921.

Sing, D. K., Désert, J.-M., Lecavelier Des Etangs, A., Ballester, G. E., Vidal-Madjar, A., Parmentier, V., Hebrard, G., Henry, G. W. (2009) Transit spectrophotometry of the exoplanet HD 189733b. I. Searching for water but finding haze with HST NICMOS. *Astronomy and Astrophysics 505*, 891-899.

Snellen, I. A. G., de Mooij, E. J. W., Albrecht, S. (2009) The

changing phases of extrasolar planet CoRoT-1b. *Nature 459*, 543-545.

Southworth, J., Wheatley, P. J., Sams, G. (2007) A method for the direct determination of the surface gravities of transiting extrasolar planets. *Mon. Not. Roy. Astr. Soc. 379*, L11-L15.

Southworth, J. (2008) Homogeneous studies of transiting extrasolar planets. I. Light-curve analyses. *Mon. Not. Roy. Astr. Soc. 386*, 1644-1666.

Southworth, J. (2009) Homogeneous studies of transiting extrasolar planets - II. Physical properties. *Monthly Notices of the Royal Astronomical Society 394*, 272-294.

Stello, D., and 24 colleagues (2009) Radius Determination of Solar-type Stars Using Asteroseismology: What to Expect from the Kepler Mission. *Astroph. J. 700*, 1589-1602.

Sterne, T. E. 1940. On the Determination of the Orbital Elements of Eccentric Eclipsing Binaries. *Proc. Nat. Ac. Sci. 26*, 36-40.

Struve, O. (1952) Proposal for a project of high-precision stellar radial velocity work. *The Observatory 72*, 199-200.

Swain, M. R., Vasisht, G., Tinetti, G. (2008) The presence of methane in the atmosphere of an extrasolar planet. *Nature 452*, 329-331.

Swain, M. R., Vasisht, G., Tinetti, G., Bouwman, J., Chen, P., Yung, Y., Deming, D., Deroo, P. (2009) Molecular Signatures in the Near-Infrared Dayside Spectrum of HD 189733b. *Astrophys. J. 690*, L114-L117.

Tamuz, O., Mazeh, T., Zucker, S. (2005) Correcting systematic effects in a large set of photometric light curves. *Monthly Notices of the Royal Astronomical Society 356*, 1466-1470.

Tinetti, G., and 12 colleagues (2007) Water vapour in the atmosphere of a transiting extrasolar planet. *Nature 448*, 169-171.

Torres, G., Winn, J. N., Holman, M. J. (2008) Improved Parameters for Extrasolar Transiting Planets. *Astrophys. J. 677*, 1324-1342.

Torres, G., and 15 colleagues (2007) HAT-P-3b: A Heavy-Element-rich Planet Transiting a K Dwarf Star. *Astrophys. J. 666*, L121-L124.

Udalski, A., Paczynski, B., Zebrun, K., Szymanski, M., Kubiak, M., Soszynski, I., Szewczyk, O., Wyrzykowski, L., Pietrzynski, G. (2002) The Optical Gravitational Lensing Experiment. Search for Planetary and Low-Luminosity Object Transits in the Galactic Disk. Results of 2001 Campaign. *Acta Astronomica 52*, 1-37.

Vidal-Madjar, A., Lecavelier des Etangs, A., Désert, J.-M., Ballester, G. E., Ferlet, R., Hébrard, G., Mayor, M. (2003) An extended upper atmosphere around the extrasolar planet HD209458b. *Nature 422*, 143-146.

Weldrake, D. T. F., Sackett, P. D., Bridges, T. J., Freeman, K. C. (2005) An Absence of Hot Jupiter Planets in 47 Tucanae: Results of a Wide-Field Transit Search. *Astroph. J. 620*, 1043-1051.

Winn, J. N., Holman, M. J., Roussanova, A. (2007a) The Transit Light Curve Project. III. Tres Transits of TrES-1. *Astrophysical Journal 657*, 1098-1106.

Winn, J. N., and 10 colleagues (2007b) The Transit Light Curve Project. V. System Parameters and Stellar Rotation Period of HD 189733. *Astronomical Journal 133*, 1828-1835.

Winn, J. N., Henry, G. W., Torres, G., Holman, M. J. (2008) Five New Transits of the Super-Neptune HD 149026b. *Astrophysical Journal 675*, 1531-1537.

Winn, J. N., and 10 colleagues (2009a) On the Spin-Orbit Misalignment of the XO-3 Exoplanetary System. *Astrophysical Journal 700*, 302-308.

Winn, J. N., Johnson, J. A., Albrecht, S., Howard, A. W., Marcy, G. W., Crossfield, I. J., Holman, M. J. (2009b) HAT-P-7: A Retrograde or Polar Orbit, and a Third Body. *Astrophysical Journal 703*, L99-L103.

Young, A. T. (1967) Photometric error analysis. VI. Confirmation of Reiger's theory of scintillation. *Astronomical Journal 72*, 747.

Zahnle, K., Marley, M. S., Freedman, R. S., Lodders, K., Fortney, J. J. (2009) Atmospheric Sulfur Photochemistry on Hot Jupiters. *Astrophysical Journal 701*, L20-L24.